Bifurcation on the Visual Cortex with Weakly Anisotropic Lateral Coupling[*]

Martin Golubitsky[†], Lie June Shiau[‡], and Andrei Török[†]

Abstract. Mathematical studies of drug induced geometric visual hallucinations include three components: a model (or class of models) that abstracts the structure of the primary visual cortex V1; a mathematical procedure for finding geometric patterns as solutions to the cortical models; and a method for interpreting these patterns as visual hallucinations.

Ermentrout and Cowan used the Wilson–Cowan equations to model the evolution of an activity variable $a(\mathbf{x})$ that represents, for example, the voltage potential a of the neuron located at point $\mathbf{x}$ in V1. Bressloff, Cowan, Golubitsky, Thomas, and Wiener generalize this class of models to include the orientation tuning of neurons in V1 and the Hubel and Wiesel hypercolumns. In these models, $a(\mathbf{x}, \phi)$ represents the voltage potential a of the neuron in the hypercolumn located at $\mathbf{x}$ and tuned to direction ϕ. The work of Bressloff et al. assumes that lateral connections between hypercolumns are *anisotropic*; that is, neurons in neighboring hypercolumns are connected only if they are tuned to the same orientation and then only if the neurons are oriented in the cortex along the direction of their cells' preference. In this work, we first assume that lateral connections are *isotropic*: neurons in neighboring hypercolumns are connected whenever they have the same orientation tuning. Wolf and Geisel use such a model to study development of the visual cortex. Then we consider the effect of perturbing the lateral couplings to be weakly anisotropic.

There are two common features in these models: the models are continuum models (neurons and hypercolumns are idealized as points and circles), and the models all have planar Euclidean $\mathbf{E}(2)$-symmetry (when cortical lateral boundaries are ignored). The approach to pattern formation is also common. It is assumed that solutions are spatially periodic with respect to a fixed planar lattice and that patterns are formed by symmetry-breaking bifurcations (corresponding to wave vectors of shortest length) from a spatially uniform state. There are also substantial differences. In the Ermentrout–Cowan model, $\mathbf{E}(2)$ acts in its standard representation on $\mathbf{R}^2$, whereas in the Bressloff et al. model, $\mathbf{E}(2)$ acts on $\mathbf{R}^2 \times \mathbf{S}^1$ via the *shift-twist* action. In our model, isotropic coupling introduces an additional $\mathbf{S}^1$-symmetry. Weak anisotropy is then thought of as a small forced symmetry-breaking from $\mathbf{E}(2)\dot{+}\mathbf{S}^1$ to $\mathbf{E}(2)$ in its shift-twist action.

The bifurcation analyses in each of these theories proceed along similar lines, but each produces different hallucinatory images—many of which have been reported in the psychophysics literature. The Ermentrout–Cowan model produces spirals and funnels, whereas the Bressloff et al. model produces in addition thin line images including honeycombs and cobwebs. Finally, our model produces three types of time-periodic states: rotating structures such as spirals, states that appear to rush

---

[†]Department of Mathematics, University of Houston, Houston, TX 77204-3008 (mg@uh.edu, torok@math.uh.edu).

[‡]Department of Mathematics, University of Houston - Clear Lake, Houston, TX 77058 (shiau@cl.uh.edu).

into (or out from) a tunnel with its hole in the center of the visual field, and pulsating images. Although it is known that branches of time-periodic states can emanate from steady-state bifurcations in systems with symmetry, this model provides the first examples of this phenomena in a specific class of models.

Key words. bifurcation, pattern formation, symmetry, hallucinations, visual cortex, rotating waves

AMS subject classifications. 37G40, 34C23, 92C15

PII. S1111111102409882

---

1. Introduction and overview. In the 1930's, Klüver classified geometric visual hallucinations into four groups of *form constants* (see [17, p. 66]): honeycombs, cobwebs, tunnels, and spirals. Klüver states "For the sake of analysis in terms of 'form,' we have ignored aspects of color, brightness, and movement" and, on p. 71, "We wish to stress merely one point, namely, that under diverse conditions the visual system responds in terms of a limited number of form constants."

Ermentrout and Cowan [9] pioneered an approach to the mathematical study of geometric patterns produced in drug induced hallucinations. They assumed that the drug uniformly stimulates an inactive cortex and produces, by spontaneous symmetry-breaking, a patterned activity state. The mind then interprets the pattern as a visual image—namely, the visual image that would produce the same pattern of activity on the primary visual cortex V1.[1] The Ermentrout–Cowan analysis assumes that a differential equation governs the symmetry-breaking transition from an inactive to an active cortex and then studies the transition abstractly using standard pattern formation arguments developed for reaction-diffusion equations. Their cortical patterns are obtained by thresholding. (Points where the solution is greater than some threshold are colored black, whereas all other points are colored white.) These cortical patterns are then transformed to retinal patterns[2] using the inverse of the retino-cortical map described below (see (1.4)), and these retinal patterns are similar to some of the geometric patterns of visual hallucinations, namely, tunnels and spirals.

It is now well established that neurons in V1 are sensitive to orientations in the visual field,[3] and it is mathematically reasonable to assign an orientation preference to each neuron in V1. Hubel and Wiesel [16] introduced the notion of a *hypercolumn*—a region in V1 containing

---

[1]The *primary visual cortex*, or V1, is the area of the visual cortex that receives electrical signals directly from the retina.

[2]The *retina* is the light-sensitive tissue lining the back of the eyeball that sends electrical impulses to the brain.

[3]Experiments show that most V1 cells signal the local orientation of a contrast edge or bar; these neurons are tuned to a particular local orientation. See [16, 12, 2, 4] and [6] for more discussion.

for each orientation at a single point in the visual field (a mathematical idealization) a neuron sensitive to that orientation.

More recently, Bressloff et al. [6] studied the geometric patterns of drug induced hallucinations by including orientation sensitivity. As before, the drug stimulation is assumed to induce spontaneous symmetry-breaking, and the analysis is local in the sense of bifurcation theory. There is one major difference between the approaches in [6] and [9]. Ignoring lateral boundaries, Ermentrout and Cowan [9] idealize the cortex as a plane, whereas Bressloff et al. [6] take into account the orientation tuning of cortical neurons and idealize the cortex as $\mathbf{R}^2 \times \mathbf{S}^1$. This approach leads to a method for recovering thin line hallucinations such as cobwebs and honeycombs in addition to the threshold patterns found in the Ermentrout–Cowan theory.

There are two types of connections between neurons in V1: local and lateral. Experimental evidence suggests that neurons within a hypercolumn are all-to-all connected, whereas neurons in different hypercolumns are connected in a very structured way. This structured lateral coupling is called *anisotropic*, and it is the bifurcation theory associated with anisotropic coupling that is studied in Bressloff et al. [6, 5].

In this paper, we study generic bifurcations when lateral coupling is weakly anisotropic. First, we study bifurcations in models that are isotropic, showing that these transitions lead naturally to a richer set of planforms than is found in [6, 5] and, in particular, to time-periodic states. (Isotropic models have an extra $\mathbf{S}^1$-symmetry and have been studied by Wolf and Geisel [26] as a model for the development of anisotropic lateral coupling.) There are three types of time dependent solutions: slowly *rotating* spiral and funnel shaped retinal images; *tunneling* images, where the retinal image appears to rush into or spiral into the center of the visual field; and *pulsating* images, where the spatial pattern of the solution changes periodically in time. Such images have been reported in the psychophysics literature; see Klüver [17, p. 24]. (Note that near death experiences are sometimes described as traveling down a tunnel toward a central area.) Second, we consider weak anisotropy as forced symmetry-breaking from isotropy and by doing so find two additional rotating time-periodic states.

We note that time-periodic, spatially periodic states have been studied previously in Tass [24] using averaging (Hopf bifurcation) applied to the Ermentrout–Cowan activator-inhibitor model [9], whereas our results lead to time-periodic states through symmetry-breaking steady-state bifurcations.

We mention two caveats associated with our methods. First, our analysis applies only to generic members of the general class of equations having symmetries associated to isotropic lateral coupling (and to weak symmetry-breakings that preserve the symmetry of anisotropic lateral coupling). It would be an extraordinarily difficult calculation to show, for example,

that every statement that we make is valid for some particular variant of the Wilson–Cowan equations, though most likely they are valid. Second, we assume that the new states are hyperbolic (which is true generically but is also quite difficult to verify in a particular model).

The remainder of this section is devoted to two primary issues: the background from previous studies that is needed to understand the current study and the comparison of our results (on the square lattice) with previous results. The section ends with a brief description of the (more complicated) hexagonal lattice results.

1.1. The continuum models and cortical planforms. The Ermentrout and Cowan [9] model of V1 consists of neurons located at each point $\mathbf{x}$ in $\mathbf{R}^2$. Their model equations, variants of the Wilson–Cowan equations [25], are written in terms of a real-valued *activity variable* $a(\mathbf{x})$, where a represents, say, the voltage potential of the neuron at location $\mathbf{x}$.

Bressloff et al. [6] incorporate the Hubel–Weisel hypercolumns [16] into their model of V1 by assuming that there is a hypercolumn centered at each location $\mathbf{x}$. Here a *hypercolumn* denotes a region of cortex that contains neurons sensitive to orientation ϕ for each direction ϕ. Their models, also adaptations of the Wilson–Cowan equations [25], are written in terms of a real-valued *activity variable* $a(\mathbf{x}, \phi)$, where a represents, say, the voltage potential of the neuron tuned to orientation ϕ in the hypercolumn centered at location $\mathbf{x}$. Note that angles ϕ and $\phi + \pi$ give the same orientation; so

$$a(\mathbf{x}, \phi + \pi) = a(\mathbf{x}, \phi).$$

The cortical planform associated to $a(\mathbf{x}, \phi)$ is obtained in a way that is different from the Ermentrout–Cowan approach. For each fixed $\mathbf{x} \in \mathbf{R}^2$, $a(\mathbf{x}, \cdot)$ is a function on the circle. The planform associated to a is obtained through a *winner-take-all* strategy. The neuron that is most active in its hypercolumn is presumed to suppress the activity of other neurons within that hypercolumn. The winner-take-all strategy chooses, for each $\mathbf{x}$, the directions ϕ that maximize $a(\mathbf{x}, \cdot)$ and results in a field of directions. The two approaches to creating planforms can be combined by assigning directions only to those locations $\mathbf{x}$ where the associated maximum of $a(\mathbf{x}, \cdot)$ is larger than a given threshold.

A possible justification for the continuum model that idealizes a hypercolumn at each cortex location is that each location is in fact surrounded by neurons sensitive to all of the possible orientations. This fact suggests that the signal read from the primary visual cortex V1 need not be limited to one orientation from each "physical" hypercolumn. In V1, there is a grid of physical hypercolumns that is approximately 36×36 in extent. (See [5] and references therein.) It is reasonable to suppose that other layers of the visual cortex receive much more information than a 36×36 matrix of orientation values.
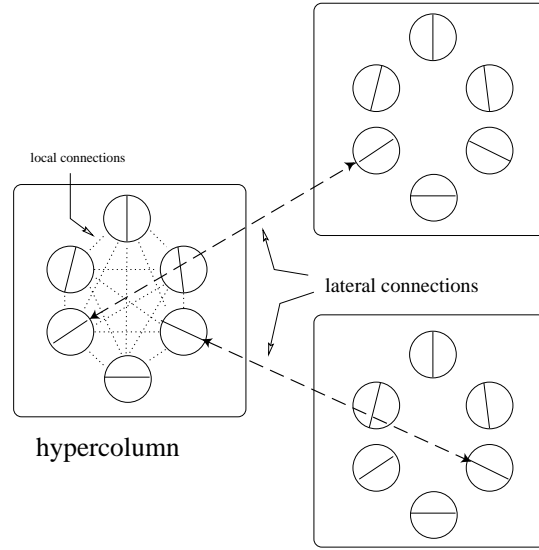
Figure 1. *Illustration of isotropic local and anisotropic lateral connection patterns.*

1.2. Euclidean symmetry. The Euclidean group $\mathbf{E}(2)$ is crucial to the analyses in both [9] and [6], but the way that group acts is different. In Ermentrout and Cowan, the Euclidean group acts on the plane by its standard action, whereas in Bressloff et al., the Euclidean group acts on $\mathbf{R}^2 \times \mathbf{S}^1$ by the so-called shift-twist representation, as we now explain.

Bressloff et al. [6] argue, based on experiments by Blasdel [2] and Eysel [10], that the lateral connections between neurons in neighboring hypercolumns are *anisotropic*. That anisotropy states that the *strength* of the connections between neurons in two neighboring hypercolumns depends on the orientation tuning of both neurons and on the relative locations of the two hypercolumns. Moreover, this anisotropy is idealized to the one illustrated in Figure 1, where only neurons with the same orientation selectivity are connected and then only neurons that are oriented along the direction of their cells preference are connected. These conclusions are based on work of Gilbert [12] and Bosking et al. [4]. In particular, the symmetries of V1 model equations are those that are consistent with the idealized structure shown in Figure 1.

The Euclidean group $\mathbf{E}(2)$ is generated by translations, rotations, and a reflection. The action of $\mathbf{E}(2)$ on $\mathbf{R}^2 \times \mathbf{S}^1$ that preserves the structure of lateral connections illustrated in Figure 1 is the *shift-twist* action. This action is given by

$$
\begin{aligned}
\mathcal{T}_{\mathbf{y}}(\mathbf{x}, \phi) &\equiv (\mathbf{x} + \mathbf{y}, \phi), \\
\mathcal{R}_{\theta}(\mathbf{x}, \phi) &\equiv (R_{\theta}\mathbf{x}, \phi + \theta), \\
\mathcal{M}_{\kappa}(\mathbf{x}, \phi) &\equiv (\kappa\mathbf{x}, -\phi),
\end{aligned}
$$

(1.1)

where $(\mathbf{x}, \phi) \in \mathbf{R}^2 \times \mathbf{S}^1$, $\mathbf{y} \in \mathbf{R}^2$, κ is the reflection $(x_1, x_2) \mapsto (x_1, -x_2)$, and $R_{\theta} \in \mathbf{SO}(2)$ is the rotation of the plane counterclockwise through angle θ.
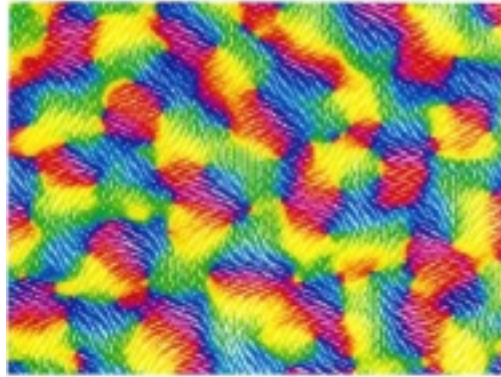
Figure 2. *Distribution of orientation preferences in the Macaque V1 obtained via optical imaging and using color to indicate iso-orientation patches. Redrawn from* [2].
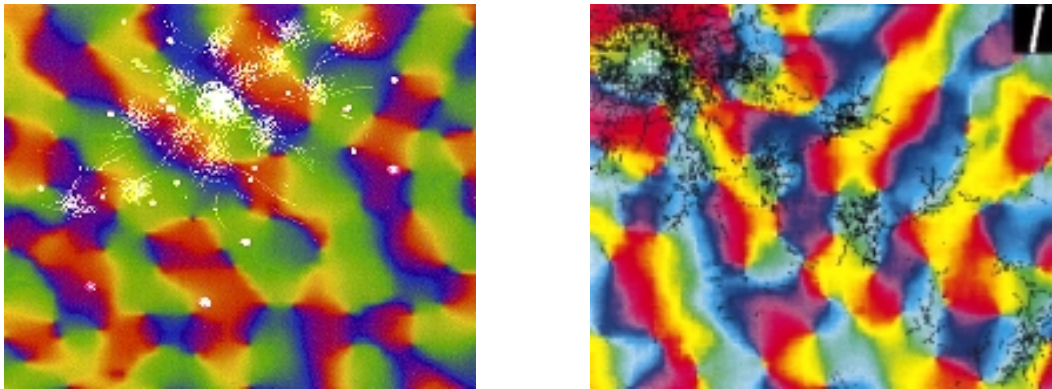
Figure 3. *Lateral connections made by cells in Macaque (left panel) and Tree Shrew (right panel) V1. A radioactive tracer is used to show the locations of all terminating axons from cells in a central injection site, superimposed on an orientation map obtained by optical imaging. Redrawn from* [23] *and* [4].

Work on optical imaging has made it possible to see how the orientation preferences of cells are actually distributed in V1 [2], and a variety of stains and labels have made it possible to see how they are interconnected [10, 4]. Figure 2 shows the distribution of orientation preferences in the Macaque. In particular, approximately every millimeter there is an *iso-orientation patch* of a given preference.

Recent optical imaging experiments combined with anatomical tracer injections suggest that there is a spatial anisotropy in the distribution of patchy horizontal connections, as illustrated in Figure 3. It will be seen from the right panel that the anisotropy is particularly pronounced in the tree shrew. The major axis of the horizontal connections tends to run parallel to the visuotopic axis of the connected cells' common orientation preference. There is also a clear anisotropy in the patchy connections of the Macaque, as seen in the left panel.
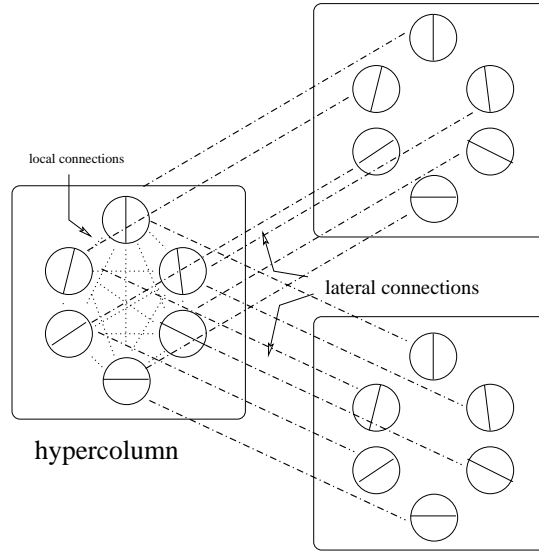
Figure 4. *Illustration of isotropic local and isotropic lateral connection patterns.*

However, in this case, most of the anisotropy can be accounted for by the fact that there is a stretching in the direction orthogonal to ocular dominance columns [1, 23]. It is possible that when this stretching is factored out, there remains a weak anisotropy correlated with orientation selectivity, but this remains to be confirmed experimentally. It should further be noted that feedback connections from higher cortical areas are also patchy and appear to link cells with similar functional features. Preliminary studies suggest that these feedback connections do seem to have a much stronger anisotropy than the lateral connections [1]. This is still a matter of ongoing investigation.

1.3. Isotropy of lateral connections. As noted in the previous paragraph, the anisotropy in lateral connections pictured in Figure 1 can be small in the following sense. We call the lateral connections between hypercolumns *isotropic*, as is done in Wolf and Geisel [26], if the strength of lateral connections between neurons in two neighboring hypercolumns depends only on the difference between the angles of the neurons' orientation sensitivity. Lateral connections in the isotropic model are illustrated in Figure 4. In this model, equations admit, in addition to Euclidean symmetry, the following $\mathbf{S}^1$-symmetry:

$$(1.2) \qquad\qquad \mathcal{I}_{\widehat{\phi}}(\mathbf{x}, \phi) = (\mathbf{x}, \phi + \widehat{\phi}).$$

Note that $\widehat{\phi} \in \mathbf{S}^1$ commutes with $\mathbf{y} \in \mathbf{R}^2$ and $R_\theta \in \mathbf{SO}(2)$, but $\kappa\widehat{\phi} = (-\widehat{\phi})\kappa$.

The action of $\gamma \in \mathbf{E}(2)\dot{+}\mathbf{S}^1$ on the activity function a is given by

$$\gamma a(\mathbf{x}, \phi) = a(\gamma^{-1}(\mathbf{x}, \phi)).$$

For example, $R_\theta \in \mathbf{SO}(2)$ acts by

$$(\mathcal{R}_\theta a)(\mathbf{x}, \phi) = a(R_{-\theta}\mathbf{x}, \phi - \theta).$$

In this paper, we determine solutions to symmetry-breaking bifurcations in the isotropic case and then study how these solutions change when anisotropy is introduced as a small forced symmetry-breaking parameter.

1.4. Symmetry-breaking bifurcations on lattices. Spontaneous symmetry-breaking in the presence of a noncompact group such as the Euclidean group is far from completely understood. The standard approach is to reduce the technical difficulties by looking only for solutions that are spatially doubly periodic with respect to some planar lattice (see Golubitsky and Stewart [13]); this is the approach taken in [9, 6] and in this study. This approach is justified by the remarkable similarities between the geometric patterns obtained mathematically in [9, 6] and the hallucinatory images reported in the scientific literature [6, 7].

The first step in such an analysis is to choose a lattice type; in this paper, we describe transitions on both the square and hexagonal lattices. The second step is to decide on the size of the lattice. Euclidean symmetry guarantees that at bifurcation, critical eigenfunctions will have *plane wave* factors $e^{2\pi i \mathbf{k} \cdot \mathbf{x}}$ for some critical dual wave vector $\mathbf{k}$. See [5] or [13, Chapter 5]. Typically, the lattice size is chosen so that the critical wave vectors will be the vectors of shortest length in the dual lattice; that is, the lattice has the smallest possible size that can support doubly periodic solutions.

By restricting the bifurcation problem to a lattice, the group of symmetries is transformed to a compact group. First, translations in $\mathbf{E}(2)$ act modulo the spatial period (which we can take to be 1 on the square lattice) and thus act as a 2-torus $\mathbf{T}^2$. Second, only those rotations and reflections in $\mathbf{E}(2)$ that preserve the lattice (namely, the holohedry $\mathbf{D}_4$ for the square lattice) are symmetries of the lattice restricted problem. Thus the symmetry group of the square lattice problem is $\Gamma = \mathbf{D}_4 \dot{+} \mathbf{T}^2$. Recall that at bifurcation Γ acts on the kernel of the linearization, and a subgroup of Γ is *axial* if its fixed-point subspace in that kernel is one-dimensional. Solutions are guaranteed by the Equivariant Branching Lemma (see [14, 13]), which states the following: generically there are branches of equilibria to the nonlinear differential equation for every axial subgroup of Γ. The nonlinear analysis in [5, 9] proceeds in this fashion.

1.5. Previous results on the square lattice. In Ermentrout and Cowan [9], translation symmetry leads to eigenfunctions that are linear combinations of plane waves and, on the square lattice, to two axial planforms: stripes and squares. See Figure 5.

In Bressloff et al. [6, 5], translation symmetry leads to critical eigenfunctions that are linear combinations of functions of the form $u(\phi)e^{2\pi i \mathbf{k} \cdot \mathbf{x}}$. These eigenfunctions correspond to
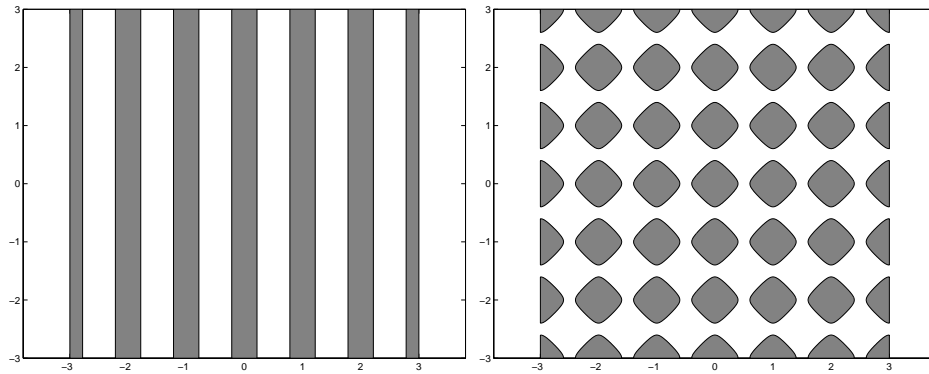
**Figure 5.** *Thresholding of eigenfunctions: (left) stripes; (right) squares.*

one of two types of representations of $\mathbf{E}(2)$ (restricted to the lattice): *scalar* (u even in ϕ) and *pseudoscalar* (u odd). The fact that two different representations of the Euclidean group can appear in bifurcations was first noted by Bosch Vivancos, Chossat, and Melbourne [3]. Bressloff et al. [6] also show that a trivial solution to the Wilson–Cowan equation will lose stability via a scalar or pseudoscalar bifurcation depending on the exact form of the lateral coupling. Thus each of these representations is, from a mathematical point of view, equally likely to occur. On the square lattice, [3, 5] show that there are two axial planforms each in the scalar and pseudoscalar cases: stripes and squares.

To picture the planforms in these cases, we must specify the function $u(\phi)$, and this can be accomplished by assuming that anisotropy is small. When anisotropy is zero, the $\mathbf{S}^1$-symmetry in (1.2) forces $u(\phi) = \cos(2m\phi)$ in the scalar case and $u(\phi) = \sin(2m\phi)$ in the pseudoscalar case. (This point will be discussed in more detail when we review representation theory in sections 2 and 4.) The assumptions in Bressloff et al. [6] imply that u is a small perturbation of sine or cosine. Note that the Ermentrout–Cowan planforms are recovered in the scalar case when $m = 0$; in this case, u is constant, and all directions are equally active. As often happens in single equation models, the first instability of a trivial (spatially constant) solution is to eigenfunctions with m small, and that is what occurs in certain models based on the Wilson–Cowan equation (see [6]). Planforms for the scalar and pseudoscalar planforms when $m = 1$ are shown in Figures 6 and 7.

1.6. New planforms when lateral connections are isotropic. In our analysis of the isotropic case ($\widetilde{\Gamma} = \Gamma \dot{+} \mathbf{S}^1$-symmetry), we find four axial subgroups (Σ_1–Σ_4) and one maximal isotropy subgroup Σ_5 with a two-dimensional fixed-point subspace. The axial subgroups lead to group orbits of equilibria. This fact must be properly interpreted to understand how the new planforms relate to the old. A phase shift of $\sin(2\phi)$ yields $\cos(2\phi)$. Thus the extra $\mathbf{S}^1$-symmetry based on isotropic lateral connections identifies scalar and pseudoscalar plan-
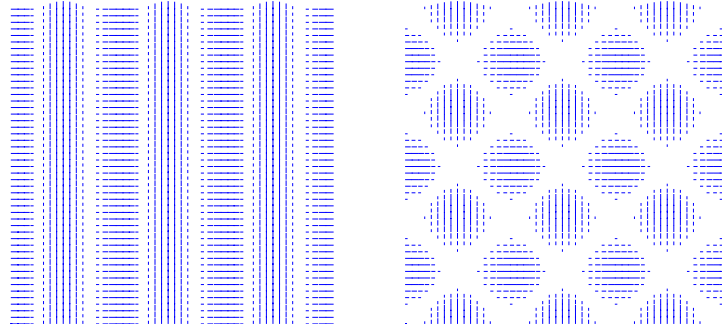
Figure 6. *Direction fields of scalar eigenfunctions: (left) stripes Σ_3; (right) squares Σ_1.*
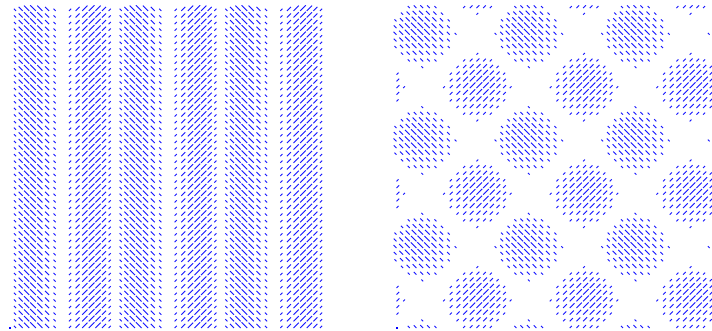
Figure 7. *Direction fields of pseudoscalar eigenfunctions: (left) stripes Σ_3; (right) squares Σ_1.*
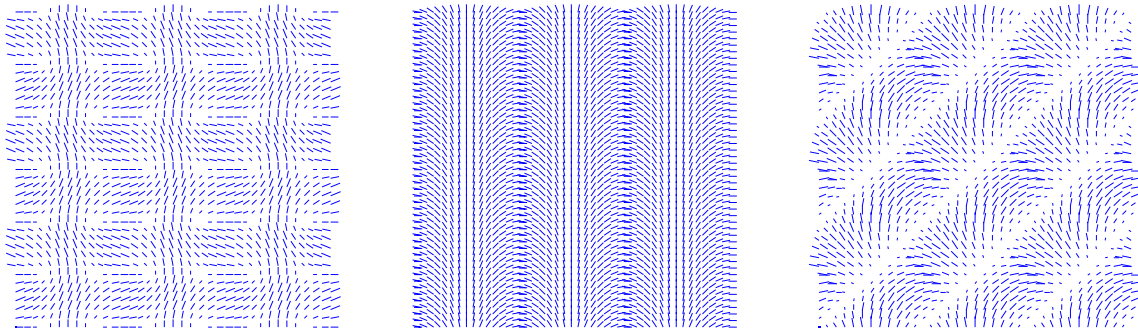
Figure 8. *Direction fields of new planforms in isotropic model: (left) axial planform Σ_2; (center) axial planform Σ_4; (right) rotating wave Σ_5 (direction of movement is up and to the left).*

forms; up to this new symmetry, the planforms are the same. Thus the axial subgroup Σ_3 corresponds to stripes (both scalar and pseudoscalar), and the axial subgroup Σ_1 corresponds to squares (both scalar and pseudoscalar). The axial subgroups Σ_2 and Σ_4 correspond to new types of planforms. Finally, the maximal isotropy subgroup Σ_5 with its two-dimensional fixed-point subspace leads to a time-periodic rotating wave whose frequency is zero at bifurcation. The planforms associated with these new types of solutions are pictured in Figure 8.

It is unusual for a steady-state bifurcation (eigenvalues of a linearization moving through 0) to lead to time-periodic states. It is well known that in systems without symmetry, time-periodic states will appear in unfoldings of codimension two Takens–Bogdanov singularities (a double zero eigenvalue with a nilpotent normal form). It is less well known that codimension one steady-state bifurcations with symmetry can also lead to time-periodic states. Field and Swift [11] were the first to find such a bifurcation (in a system with finite symmetry). Melbourne [21] was the first to find an example of a rotating wave in a steady-state bifurcation in a system with continuous symmetry. Nevertheless, the documented cases where time-periodic states occur in codimension one steady-state bifurcations are relatively rare, and our work provides the first example where this mathematical phenomenon appears in model equations.

1.7. Weak anisotropy in lateral connections. Next, we discuss what happens to the bifurcating solutions to the isotropic nonlinear equation when anisotropy is added as a small symmetry-breaking parameter. As was noted in Bressloff et al. [6], the linear effect of anisotropy is to split the eigenfunctions into scalar and pseudoscalar representations. The effect on solutions to the nonlinear equation can also be established using the methods of Lauterbach and Roberts [20]. This method is applied independently to each branch of (group orbits of) solutions found in the isotropic case. The results for square lattice solutions are easily described.

Generically, the dynamics on the $\widetilde{\Gamma}$ group orbit of equilibria corresponding to the axial subgroup Σ_3 has two (smaller Γ) group orbits of equilibria: scalar stripes and pseudoscalar stripes. There may be other equilibria coming from the $\widetilde{\Gamma}$ group orbit, but, at the very least, scalar and pseudoscalar stripes always remain as solutions.

Similarly, the dynamics on the group orbit of equilibria corresponding to the axial subgroup Σ_1 generically has two equilibria corresponding to scalar and pseudoscalar squares.

The dynamics on the group orbit of the axial subgroups Σ_2 and Σ_4 and the fifth maximal isotropy subgroup Σ_5 does not change substantially when anisotropy is added. These group orbits still remain as equilibria and rotating waves.

1.8. Retinal images. Finally, we discuss the geometric form of the cortical planforms in the visual field; that is, we try to picture the corresponding visual hallucinations. It is known that the density of neurons in the visual cortex is uniform, whereas the density of neurons in the retina falls off from the fovea[4] at a rate of $1/r^2$. Schwartz [22] observed that there is a unique conformal map taking a disk with $1/r^2$ density to a rectangle with uniform density, namely, the complex logarithm. This is also called the *retino-cortical* map. It is thought that using

---

[4]The *fovea* is the small central area of the retina that gives the sharpest vision.

the inverse of the retino-cortical map, the complex exponential, to push forward the activity pattern from V1 to the retina is a reasonable way to form the hallucination image—and this is the approach used in Ermentrout and Cowan [9] and in Bressloff et al. [6, 7]. Specifically, the transformation from polar coordinates (r, θ) on the retina to cortical coordinates (x, y) is given in Cowan [8] to be

$$
\begin{aligned}
x &= \tfrac{1}{\varepsilon} \ln \left(\tfrac{1}{\omega} r \right), \\
y &= \tfrac{1}{\varepsilon} \theta,
\end{aligned}
\tag{1.3}
$$

where ω and ε are constants. See Bressloff et al. [7] for a discussion of the values of these constants. The inverse of the retino-cortical map (1.3) is

$$
\begin{aligned}
r &= \omega \exp(\varepsilon x), \\
\theta &= \varepsilon y.
\end{aligned}
\tag{1.4}
$$

In our retinal images, we take

$$
\omega = \frac{30}{e^{2\pi}} \quad \text{and} \quad \varepsilon = \frac{2\pi}{n_h},
$$

where n_h is the number of hypercolumn widths in the cortex, which we take to be 36.

There are additional issues that need to be discussed.

1. What is the relationship between the spatial period of the planform and the size of a "physical" hypercolumn?
2. How many points within a hypercolumn should be used to create the visual image?
3. In our symmetry analysis, states are enumerated up to symmetry. Are the retinal images of symmetry-related cortical states the same?

We discuss each of these questions in turn.

1.8.1. Spatial period. The human visual cortex contains a grid of approximately 36×36 hypercolumns. Bressloff et al. [6, 7] argue that each spatial period is the size of two hypercolumns. This conclusion is based on the properties of reported visual hallucinations and on the responses of human subjects to perceived grating patterns.

1.8.2. Grid points per hypercolumn. There are regions within a fundamental square in which the line field varies continuously and curves across which discontinuities in line field direction appear. Discontinuities in the direction field follow from the winner-take-all strategy and cannot be avoided. Generally we find that to sample every region in which the line field is continuous, it is sufficient to evaluate the direction fields on a 4×4 array of points in each hypercolumn.

1.8.3. Retinal planforms from conjugate cortical planforms. We begin by justifying our choice of lattice orientation. Observe that vertical lines on the cortex are taken by (1.4) to circles in the retina. Therefore, the vertical y-direction on the cortex is a periodic direction, and it makes sense to align the square lattice so edges of the square are vertical and horizontal lines on the cortex. It is also sensible to align the hexagonal lattice so that one of the three sets of parallel lines defining a fundamental hexagon consists of horizontal lines.

Certain lattice symmetries do change the retinal planform, and some do not. Moreover, certain ways of representing the data graphically change with conjugacies, and others do not. To verify these points, consider a cortical pattern consisting of parallel stripes that is mapped by (1.4) to a concentric family of circles in the retina. Rotating this striped state on the cortex by $\pi/2$ leads to another square lattice state whose associated retinal pattern consists of radial lines. See Figures 10 (center, right) and 11 (center, right). Thus the transformation from cortex to retina given in (1.4) does not respect the symmetries of the cortex.

There are, however, certain cortical symmetries that do not change retinal planforms in any important way. First, each of the planforms that we draw has certain well-defined symmetries; indeed, our planforms are determined by these symmetries. So rotating a square symmetric cortical planform by $\pi/2$ will not change the cortical pattern and hence will not change the retinal planform. Second, translating a cortical pattern in the y-direction just rotates the retinal pattern, whereas translating a cortical pattern in the x-direction scales the retinal pattern in the radial direction. So cortical translations do not change retinal planforms in significant ways; in particular, the Klüver form constant of a retinal image is not changed by cortical translations.

Finally, note that we may draw patterns on the retina and cortex in two distinct ways. First, we may use the line fields obtained from the winner-take-all strategy; and, second, we may ignore the direction information in the line field and just fill in areas where the maximum value of $a(\mathbf{x}, \cdot)$ is greater than some threshold value, as is done in the Ermentrout–Cowan theory. The second method for representing patterns is also unchanged by symmetries in Γ that are projections of the isotropy group in $\widetilde{\Gamma}$.

The visual images that correspond to the previously derived planforms are reproduced here from Bressloff et al. [7]. Figure 9 illustrates the Ermentrout–Cowan planforms. The scalar and pseudoscalar planforms are shown in Figures 10 and 11. When these images are just thresholded, the scalar and pseudoscalar planforms are identical (since, because of $\mathbf{S}^1$-symmetry, the maximum value of $a(\mathbf{x}, \cdot)$ is the same in the corresponding planforms) and are shown in Figure 12. The new planforms found by assumption of isotropy in lateral connections are illustrated in Figures 13–15.

(a)   (b)
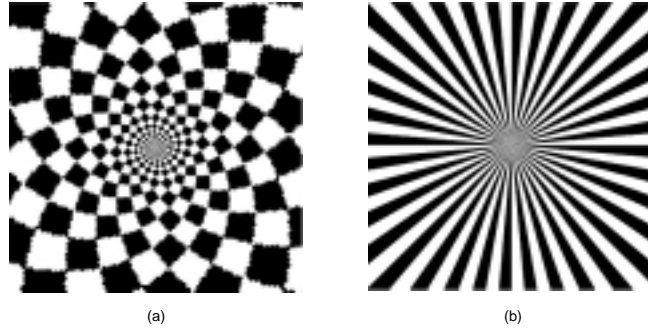
Figure 9. *Action of inverse retino-cortical map* (1.4) *on Ermentrout–Cowan noncontoured square lattice planforms:* (a) *squares;* (b) *stripes.*
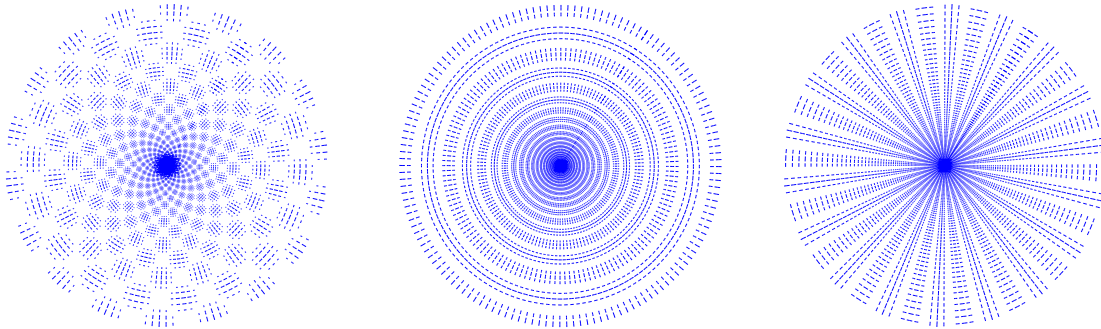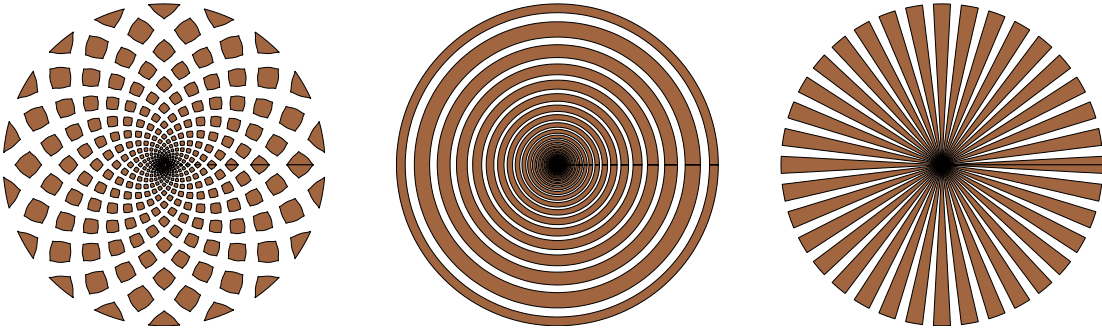

Figure 10. *Action of* (1.4) *on Bressloff* et al. *scalar square lattice planforms: (left) squares* Σ_1*; (center and right) stripes* Σ_3*.*

1.9. Hexagonal lattice planforms. In isotropic models on the hexagonal lattice, there are (at least) 12 maximal isotropy subgroups; nine of these are axial subgroups and lead to branches of group orbits of equilibria, and three of these have two-dimensional fixed-point spaces, two of which lead to rotating waves. The rotating waves look like rotating spirals in retinal coordinates. Depending on the specific model, the maximal isotropy subgroup corresponding to the third two-dimensional fixed-point space can lead to an equilibrium or a time-periodic state.

When anisotropy is added into the model, two of the nine axial solutions become time-periodic. The retinal planforms associated to these isotropy subgroups have a substantially different character—certain planforms move radially inward (or radially outward), and certain planforms spiral inward (or spiral outward). Thus rotating patterns appear in these models through spontaneous symmetry-breaking, whereas tunneling images appear through forced symmetry-breaking. All of the time-periodic patterns result from weak anisotropy, and the fact that they rotate or tunnel in the retinal image depends just on symmetry and not on the specific method by which the patterns are imaged.
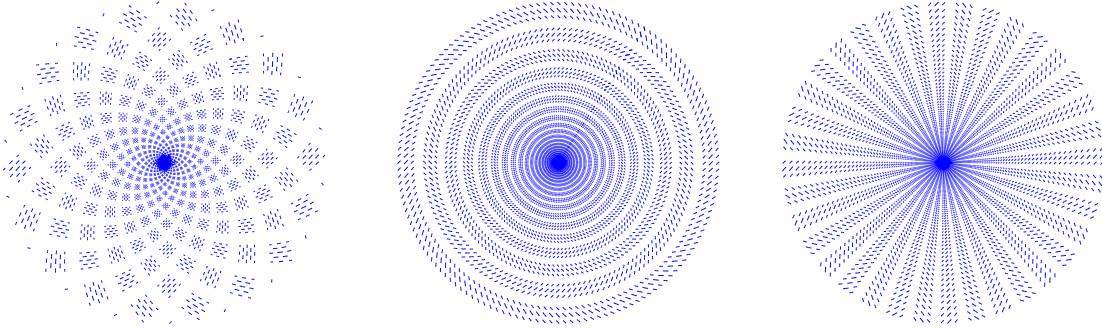
Figure 11. *Action of (1.4) on Bressloff et al. pseudoscalar square lattice planforms: (left) squares Σ_1; (center and right) stripes Σ_3.*


Figure 12. *Threshold retinal images on Bressloff et al. scalar and pseudoscalar square lattice planforms: (left) squares Σ_1; (center and right) stripes Σ_3.*

The detailed description of the square lattice results are given in section 2, and those for the hexagonal lattice are given in section 3. The proofs of the bifurcation theory statements made in these sections are deferred until section 4.

2. Square lattice planforms. In this section, we discuss the spatially doubly periodic solutions that must emanate from the simplest bifurcations of Euclidean invariant differential equations restricted to a *square* lattice. We assume that the Euclidean action on $\mathbf{R}^2 \times \mathbf{S}^1$ is the one given by (1.1) and that the extra $\mathbf{S}^1$ symmetries (1.2) associated with isotropy are present. Our findings include the following:

1. The simplest $\widetilde{\Gamma} = \Gamma \dot{+} \mathbf{S}^1$ bifurcations, where $\Gamma = \mathbf{D}_4 \dot{+} \mathbf{T}^2$, occur at irreducible representations of $\widetilde{\Gamma}$ that are the direct sum of the scalar and pseudoscalar bifurcations studied in [3, 5].

2. There are five branches of (group orbits of) solutions (corresponding to maximal isotropy subgroups of $\widetilde{\Gamma}$) that must bifurcate from a trivial equilibrium: four are equilibria, and one is a slowly traveling wave in cortical coordinates (and a rotating
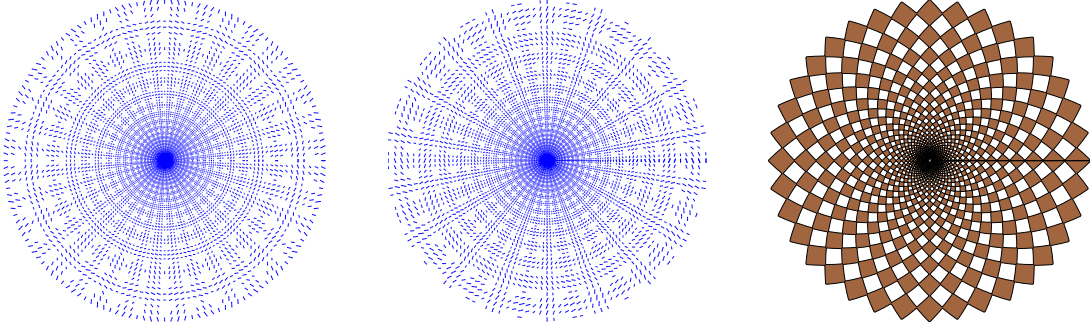
Figure 13. *New square axial planform Σ_2 in isotropic model: (left and center) conjugate line field images; (right) threshold image.*
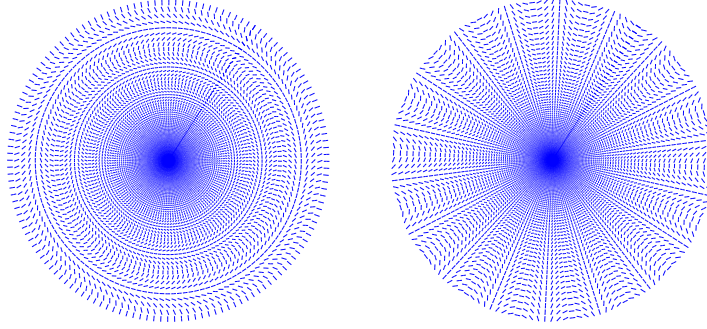
Figure 14. *New axial planform Σ_4 in isotropic model. Thresholding is not relevant for these planforms; see section 3.4.2.*

    spiral wave in retinal coordinates).

3. When weak anisotropy in the lateral connections is assumed (that is, symmetry is broken from $\widetilde{\Gamma}$ to Γ in the model equations), one solution leads to both scalar and pseudoscalar rolls (and perhaps a third intermediate state), and a second leads to both scalar and pseudoscalar squares (and perhaps a third intermediate state). The two remaining equilibria persist as equilibria when symmetry is broken, and the rotating wave also persists. These last three solution types correspond to hallucinatory states that have not been discussed previously.

In our exposition, we describe the results in this section and refer to section 4 for the details of the proofs.

2.1. Representation theory of $\widetilde{\Gamma}$. Without loss of generality, we assume that the square lattice $\mathcal{L}$ consists of squares of unit length. Let $\mathcal{F}_{\mathcal{L}}$ be the space of functions $a(\mathbf{x}, \phi)$ that are doubly periodic with respect to translations in $\mathcal{L}$ and π-periodic in ϕ. The action of $\widetilde{\Gamma}$ on $\mathcal{F}_{\mathcal{L}}$ is the one induced from the action of $\mathbf{E}(2) \dot{+} \mathbf{S}^1$ on $\mathbf{R}^2 \times \mathbf{S}^1$ given in (1.1) and (1.2).
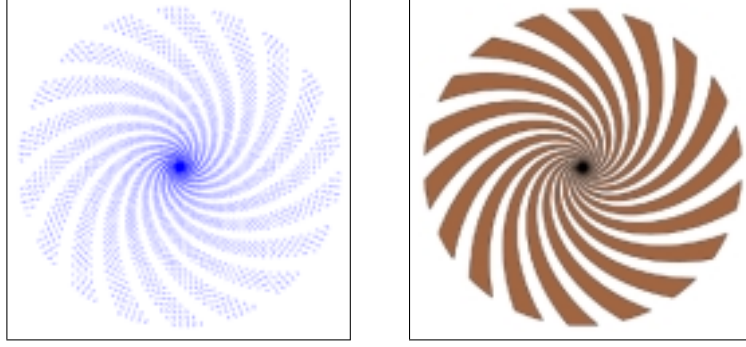
Figure 15. *Rotating planform Σ_5 in isotropic model; movies are associated to framed images.*

We expect the simplest square lattice bifurcations to be from equilibria whose linearizations have kernels that are irreducible subspaces of $\mathcal{F}_\mathcal{L}$, and we consider only bifurcations based on dual wave vectors of shortest (unit) length. It follows that we may assume that the critical eigenspace W_m consists of functions of the form

$$(2.1) \qquad a(\mathbf{x}, \phi) = \left(z_1 e^{2im\phi} + w_1 e^{-2im\phi} \right) e^{2\pi i \mathbf{k}_1 \cdot \mathbf{x}}$$
$$+ \left(z_2 e^{2im(\phi - \pi/2)} + w_2 e^{-2im(\phi - \pi/2)} \right) e^{2\pi i \mathbf{k}_2 \cdot \mathbf{x}} + c.c.,$$

where $(z_1, w_1, z_2, w_2) \in \mathbf{C}^4$. Moreover, the action of $\widetilde{\Gamma}$ on this subspace is absolutely irreducible. These statements are verified in section 4.1. From now on, for $m \geq 1$, we will identify W_m with $\mathbf{C}^4$ through (2.1).

We show in section 4.2 that, from a bifurcation theoretic point of view, we may assume that $m = 0$ or $m = 1$. The case in which $m = 0$ was considered in [5]; so, in the current analysis, we assume that $m = 1$.

In this section, we describe planforms that generically appear in bifurcations with respect to the group $\widetilde{\Gamma}$ and discuss what happens to these planforms after symmetry is broken to $\Gamma \subset \widetilde{\Gamma}$. Therefore, we are interested in how a $\widetilde{\Gamma}$ representation decomposes into Γ representations. The proof of Lemma 4.1 leads to the following lemma.

Lemma 2.1. *The subspace $W_1 \subset \mathcal{F}_\mathcal{L}$ decomposes into two nonisomorphic absolutely irreducible representations of Γ: $W_1 = W_1^+ \oplus W_1^-$, where*

$$W_1^+ = \{(u, u, v, v) \mid u, v \in \mathbf{C}\},$$
$$W_1^- = \{(u, -u, v, -v) \mid u, v \in \mathbf{C}\}.$$

The representation W_1^+ is scalar, and the representation W_1^- is pseudoscalar.

Table 1
Group action on $(z_1, w_1, z_2, w_2) \in W_1 = \mathbf{C}^4$; $\xi, \kappa \in \mathbf{D}_4$, $0 \le \theta_1, \theta_2 < 1$, and $0 \le \widehat{\phi} < \pi$.

Generators	Action
ξ	$(\overline{w}_2, \overline{z}_2, z_1, w_1)$
κ	$(w_1, z_1, \overline{z}_2, \overline{w}_2)$
$[\theta_1, \theta_2, 0]$	$(e^{2\pi i \theta_1} z_1, e^{2\pi i \theta_1} w_1, e^{2\pi i \theta_2} z_2, e^{2\pi i \theta_2} w_2)$
$\left[0, 0, \widehat{\phi}\right]$	$(e^{-2i\widehat{\phi}} z_1, e^{2i\widehat{\phi}} w_1, e^{-2i\widehat{\phi}} z_2, e^{2i\widehat{\phi}} w_2)$

2.2. Group action on W_1.

A calculation shows that when $m = 1$, $\widetilde{\Gamma}$ acts on $W_1 \cong \mathbf{C}^4$ in the way presented in Table 1. The action for general m is presented in Table 6. When $m = 1$, the action has a nontrivial kernel $\mathbf{Z}_2$ generated by $\left[\frac{1}{2}, \frac{1}{2}, \frac{\pi}{2}\right]$.

Table 2
Square lattice maximal isotropy subgroups of $\widetilde{\Gamma}$ acting on $\mathbf{C}^4$; $u \in \mathbf{C}$.

	Generators	Fixed subspace	Dim	Name
Σ_1	κ, ξ	$\mathbf{R}\{(1,1,1,1)\}$	1	squares
Σ_2	$\kappa, \left[\frac{3}{4}, \frac{1}{4}, \frac{\pi}{4}\right]\xi$	$\mathbf{R}\{(1,1,1,-1)\}$	1	
Σ_3	$\kappa, \xi^2, [0, \theta_2, 0]$	$\mathbf{R}\{(1,1,0,0)\}$	1	stripes
Σ_4	$\kappa\xi^2, [0, \theta_2, 0], [\theta_1, 0, \pi\theta_1]$	$\mathbf{R}\{(1,0,0,0)\}$	1	
Σ_5	$\kappa\xi, [\theta_1, \theta_1, \pi\theta_1]$	$\{(u, 0, \overline{u}, 0)\}$	2	rotating spirals

The relations among the generators are as follows:

$$(2.2) \qquad \begin{aligned} \xi\kappa &= \kappa\xi^{-1}, \\ \kappa[\theta_1, \theta_2, \widehat{\phi}] &= [\theta_1, -\theta_2, -\widehat{\phi}]\kappa, \\ \xi[\theta_1, \theta_2, \widehat{\phi}] &= [-\theta_2, \theta_1, \widehat{\phi}]\xi. \end{aligned}$$

The list of maximal isotropy subgroups of $\widetilde{\Gamma}$ acting on $\mathbf{C}^4$ is given in Table 2. This list is a subset of the list of isotropy subgroups of $\widetilde{\Gamma}$ acting on $\mathbf{C}^4$ given in Table 7. We discuss only those planforms associated with maximal isotropy subgroups. Table 2 shows that there are four axial subgroups (Σ_1–Σ_4) of $\widetilde{\Gamma}$ acting on W_1 and one maximal isotropy subgroup with a two-dimensional fixed-point subspace Σ_5. Note that the normalizer of Σ_5 is generated by $[\theta_1, -\theta_1, 0]$ over Σ_5.

2.3. Solutions corresponding to maximal isotropy subgroups.

The Equivariant Branching Lemma [14] proves the existence (generically) of equilibria corresponding to each axial subgroup. Generally, there is a branch of rotating waves corresponding to each maximal isotropy subgroup with a two-dimensional fixed-point subspace when the normalizer of that subgroup contains a circle group (see Melbourne [21, Theorem 2.4]). Moreover, the periods

of these solutions will tend to infinity at the bifurcation point. See section 4.4 for additional details.

Finally, we note that each of these solutions can be asymptotically stable to perturbations within the square lattice. The computation of linear stability is complicated and the calculations are not included in this paper. The results of these calculations are given in Table 8 in subsection 4.5.

2.4. The effects of weak anisotropy. We discuss how solutions corresponding to $\widetilde{\Gamma}$-bifurcations behave generically when the isotropy of the lateral connections is broken, that is, when the $\widetilde{\Gamma}$-equivariant vector field is perturbed to a Γ-equivariant field.

2.4.1. Squares: $\Sigma_1 = \mathbf{D}_4(\kappa, \xi)$. Generically, breaking the isotropy of the lateral connections leads to a bifurcation of the $\mathbf{D}_4$ steady state into scalar steady states of type Esquares (conjugate in Γ to $S_1 = (1, 1, 1, 1)$) and pseudoscalar steady states of type Osquares (conjugate in Γ to $S_2 = (1, -1, 1, -1)$). See [5, Tables 5, 8, and 11, and Figure 3]. In addition to these two types of steady states, it is possible for there to be other intermediate steady states. Details are found in section 4.6.1. See Figures 6 (right) and 7 (right) for the cortical planforms and Figures 10 (left) and 11 (left) for the associated retinal planforms.

2.4.2. $\Sigma_2 = \mathbf{D}_4(\langle \kappa, \left[\frac{3}{4}, \frac{1}{4}, \frac{\pi}{4}\right] \xi \rangle)$. The results for Σ_2 equilibria are similar to those for Σ_1 equilibria. See section 4.6.2 and Figure 13. None of these equilibria are scalar or pseudoscalar states.

2.4.3. Stripes: $\Sigma_3 = \langle \kappa, \xi^2, [0, \theta_2, 0] \rangle$. We show that generically, breaking the isotropy of the lateral connection leads to a bifurcation of this steady state into two states: a scalar steady state of type Erolls (conjugate in Γ to $R_1 = (1, 1, 0, 0)$) and a pseudoscalar steady state of type Orolls (conjugate in Γ to $R_2 = (1, -1, 0, 0)$). See [5, Tables 5, 8, and 11, and Figures 2(c,d)]. In addition to these two types of steady states, it is possible for there to be other intermediate steady states. Details are found in section 4.6.3. See Figures 6 (left) and 7 (left) for the cortical planforms and Figures 10 (center, right) and 11 (center, right) for the associated retinal planforms.

2.4.4. $\Sigma_4 = \langle \kappa \xi^2, [0, \theta_2, 0], [\theta_1, 0, \pi \theta_1] \rangle$. Steady states corresponding to Σ_4 persist as steady states under symmetry-breaking perturbations of the system and are conjugate to $T_1 = (1, 0, 0, 0)$. Details are found in section 4.6.4. See Figure 8 (center) for the cortical planform and Figure 14 for the associated retinal planforms.

2.4.5. Rotating spirals: $\Sigma_5 = \langle \kappa \xi, [\theta_1, \theta_1, \pi \theta_1] \rangle$. In section 4.4, we show that generically a branch of time-periodic rotating waves bifurcates in the fixed-point subspace of isotropy subgroup Σ_5. These rotating waves $Z(t)$ persist when symmetry is broken to Γ and up to

conjugacy have the form

$$Z(t) = [t, -t, 0](1, 0, 1, 0).$$

Details are found in section 4.6.5. See Figure 8 (right) for the cortical planform and Figure 15 for the associated retinal planform. This picture is a static image of a time-periodic rotating spiral.

3. Hexagonal lattice planforms. In this section, we discuss the spatially doubly periodic solutions that must emanate from the simplest (shortest wave vector) bifurcations of Euclidean invariant differential equations restricted to a *hexagonal* lattice. Our findings include the following:

1. There are (at least) 12 maximal isotropy subgroups in the isotropic case.
2. Three of these 12 have two-dimensional fixed-point subspaces.
3. Two of those three lead generically to rotating waves, and the third one can lead either to equilibria or to time-periodic states.
4. Weak anisotropy forces two of the nine axial solutions to be time-periodic.
5. Pseudoscalar hexagons do not appear naturally as solutions on the hexagonal lattice when weak anisotropy is present.

The group action in the smallest wave vector isotropic case is on a 12-dimensional space as shown in Table 3. The maximal isotropy subgroups are listed in Table 4.

3.1. Representation theory of $\widetilde{\Gamma}$. Without loss of generality, we assume that the hexagonal lattice $\mathcal{L}$ is generated by vectors

$$\boldsymbol{\ell}_1 = \left(1, \frac{1}{\sqrt{3}}\right) \quad \text{and} \quad \boldsymbol{\ell}_2 = \left(0, \frac{2}{\sqrt{3}}\right).$$

Generators for the dual lattice $\mathcal{L}^*$ are the unit length vectors

$$\mathbf{k}_1 = (1, 0) \quad \text{and} \quad \mathbf{k}_2 = \frac{1}{2}(-1, \sqrt{3}).$$

Let

$$\mathbf{k}_3 = -(\mathbf{k}_1 + \mathbf{k}_2) = \frac{1}{2}(-1, -\sqrt{3}).$$

Let $\mathcal{F}_{\mathcal{L}}$ be the space of functions $a(\mathbf{x}, \phi)$ that are doubly periodic with respect to translations in $\mathcal{L}$ and π-periodic in ϕ. The full symmetry group whose bifurcations we analyze is

$$\widetilde{\Gamma} = (\mathbf{D}_6 \dotplus \mathbf{T}^2) \dotplus \mathbf{S}^1.$$

The action of $\widetilde{\Gamma}$ on $\mathcal{F}_{\mathcal{L}}$ is the one induced from the action of $\mathbf{E}(2)\dot{+}\mathbf{S}^1$ on $\mathbf{R}^2 \times \mathbf{S}^1$ given in (1.1) and (1.2).

We expect the simplest hexagonal lattice bifurcations to be from equilibria whose linearizations have kernels that are irreducible subspaces of $\mathcal{F}_{\mathcal{L}}$, and we consider only bifurcations based on dual wave vectors of shortest (unit) length. It follows from these assumptions that we may assume that the critical eigenspace W_m consists of eigenfunctions of the form

$$
\begin{aligned}
a(\mathbf{x}, \phi) \;=\; & \left(z_1 e^{2im\phi} + w_1 e^{-2im\phi}\right) e^{2\pi i \mathbf{k}_1 \cdot \mathbf{x}} \\
& + \left(z_2 e^{2im(\phi - 2\pi/3)} + w_2 e^{-2im(\phi - 2\pi/3)}\right) e^{2\pi i \mathbf{k}_2 \cdot \mathbf{x}} \\
& + \left(z_2 e^{2im(\phi + 2\pi/3)} + w_2 e^{-2im(\phi + 2\pi/3)}\right) e^{2\pi i \mathbf{k}_3 \cdot \mathbf{x}} + c.c.,
\end{aligned}
$$

(3.1)

where $(z_1, w_1, z_2, w_2, z_3, w_3) \in \mathbf{C}^6$. On this subspace, the action of the group $\widetilde{\Gamma}$ is absolutely irreducible. This statement is verified in a manner entirely analogous to that of (2.1). As with the square lattice, we assume that $m = 1$ in our bifurcation analysis. The cases in which $m > 1$ are identical once one divides by the kernel of the representation, and the case in which $m = 0$ was considered in [5]. From now on, for $m \geq 1$, we will identify W_m with $\mathbf{C}^6$ through (3.1).

Lemma 3.1. *The subspace $W_1 \subset \mathcal{F}_{\mathcal{L}}$ decomposes into two nonisomorphic absolutely irreducible representations of Γ: $W_1 = W_1^+ \oplus W_1^-$, where*

$$
\begin{aligned}
W_1^+ \;&=\; \{(u, u, v, v, w, w) \mid u, v \in \mathbf{C}\}, \\
W_1^- \;&=\; \{(u, -u, v, -v, w, -w) \mid u, v \in \mathbf{C}\}.
\end{aligned}
$$

The representation W_1^+ is scalar, and the representation W_1^- is pseudoscalar. The proof is similar to that of Lemma 2.1.

3.2. Group action on W_1. A calculation leads to the group action on W_1 given in Table 3. Note that the action has a trivial kernel.

<div align="center">

Table 3

Group action on $(z_1, w_1, z_2, w_2, z_3, w_3) \in W_1 = \mathbf{C}^6$; $\xi, \kappa \in \mathbf{D}_6$, $0 \leq \theta_1, \theta_2 < 1$, and $0 \leq \widehat{\phi} < \pi$.

</div>

Generators	Action
ξ	$(\overline{w}_2, \overline{z}_2, \overline{w}_3, \overline{z}_3, \overline{w}_1, \overline{z}_1)$
κ	$(w_1, z_1, w_3, z_3, w_2, z_2)$
$[\theta_1, \theta_2, 0]$	$(e^{-2\pi i \theta_1} z_1, e^{-2\pi i \theta_1} w_1, e^{-2\pi i \theta_2} z_2, e^{-2\pi i \theta_2} w_2, e^{2\pi i(\theta_1 + \theta_2)} z_3, e^{2\pi i(\theta_1 + \theta_2)} w_3)$
$\left[0, 0, \widehat{\phi}\right]$	$(e^{-2i\widehat{\phi}} z_1, e^{2i\widehat{\phi}} w_1, e^{-2i\widehat{\phi}} z_2, e^{2i\widehat{\phi}} w_2, e^{-2i\widehat{\phi}} z_3, e^{2i\widehat{\phi}} w_3)$

Hexagonal lattice maximal isotropy subgroups: $u \in \mathbf{C}$; $v = e^{i\frac{\pi}{6}}$. The general fixed-point subspace of k-groups is $\mathbf{R}\{(v^{3k}, v^{3k}, v^{7k}, v^{11k}, v^{11k}, v^{7k})\}$.

	Generators	Fixed subspace	Dim	Normalizer
$k = 0$	κ, ξ	$\mathbf{R}\{(1, 1, 1, 1, 1, 1)\}$	1	$[0, 0, \frac{\pi}{2}]$
$k = 1$	$\kappa, [0, 0, \frac{\pi}{6}]\xi$	$\mathbf{R}\{(i, i, -v, \overline{v}, \overline{v}, -v)\}$	1	$[0, 0, \frac{\pi}{2}]$
$k = 2$	$\kappa, [0, 0, \frac{\pi}{3}]\xi$	$\mathbf{R}\{(1, 1, -v^2, iv, iv, -v^2)\}$	1	$[0, 0, \frac{\pi}{2}]$
$k = 3$	$\kappa, [0, 0, \frac{\pi}{2}]\xi$	$\mathbf{R}\{(i, i, i, i, i, i)\}$	1	$[0, 0, \frac{\pi}{2}]$
$k = 4$	$\kappa, [0, 0, \frac{2\pi}{3}]\xi$	$\mathbf{R}\{(1, 1, iv, -v^2, -v^2, iv)\}$	1	$[0, 0, \frac{\pi}{2}]$
$k = 5$	$\kappa, [0, 0, \frac{5\pi}{6}]\xi$	$\mathbf{R}\{(i, i, \overline{v}, -v, -v, \overline{v})\}$	1	$[0, 0, \frac{\pi}{2}]$
7	$\kappa\xi^3, [0, \theta_2, 0], [\theta_1, 0, -\pi\theta_1]$	$\mathbf{R}\{(1, 0, 0, 0, 0, 0)\}$	1	$[\frac{1}{2}, 0, 0]$
8	$\kappa, \xi^3, [0, \theta_2, 0], [\frac{1}{2}, 0, \frac{\pi}{2}]$	$\mathbf{R}\{(1, 1, 0, 0, 0, 0)\}$	1	$[\frac{1}{2}, 0, 0]$
9	$\xi^2, \kappa\xi, [\frac{1}{3}, \frac{1}{3}, \frac{2\pi}{3}]$	$\mathbf{R}\{(1, 0, 1, 0, 1, 0)\}$	1	$[0, 0, \frac{\pi}{2}]$
10	$\kappa\xi, [\theta_1, \theta_1, -\pi\theta_1]$	$(u, 0, \overline{u}, 0, 0, 0)$	2	$[\theta_1, -\theta_1, 0]$
11	$\kappa\xi^4, [\theta_1, -\theta_1, -\pi\theta_1]$	$(u, 0, 0, u, 0, 0)$	2	$[\theta_1, \theta_1, 0]$
12	$\kappa\xi, \xi^3, [\frac{1}{2}, \frac{1}{2}, \frac{\pi}{2}]$	$(u, \overline{u}, \overline{u}, u, 0, 0)$	2	$[0, -\frac{1}{2}, \frac{\pi}{4}]$

The relations among the generators are as follows:

$$(3.2) \quad \begin{aligned} \kappa\xi\kappa &= \xi^{-1}, \\ \kappa[\theta_1, \theta_2, \widehat{\phi}] &= [\theta_1, -\theta_1 - \theta_2, -\widehat{\phi}]\kappa, \\ \xi[\theta_1, \theta_2, \widehat{\phi}] &= [-\theta_2, \theta_1 + \theta_2, \widehat{\phi}]\xi. \end{aligned}$$

Remark 3.1. It follows from the action of $[0, 0, \widehat{\phi}]$ and Lemma 3.1 that the action of $\widetilde{\Gamma}$ on $\mathbf{C}^6$ is absolutely irreducible.

3.3. Solutions corresponding to maximal isotropy subgroups. Up to conjugacy there are (at least) 12 maximal isotropy subgroups of the action of $\widetilde{\Gamma}$ on $W_1 \cong \mathbf{C}^6$, and these are listed in Table 4. We believe that it is unlikely that there are additional maximal isotropy subgroups, but we have not been able to give a complete proof of this conjecture (see section 4.7). Nine of the maximal isotropy subgroups are axial (including a family of six that are isomorphic to $\mathbf{D}_6$); hence the Equivariant Branching Lemma [14] proves the existence (generically) of a branch of equilibria for each of them.

The other three maximal isotropy subgroups have a two-dimensional fixed-point space. Two of them have as their normalizer a circle group, and generically they lead to a rotating wave just as in the square lattice Σ_4 case. See section 4.4. The remaining one has $\mathbf{Z}_4$ as its normalizer and can lead either to equilibria or to time-periodic discrete rotating waves, as discussed in section 3.4.7.

The cortical and retinal planforms associated to each of these maximal isotropy subgroups are presented in Figures 16–28. In these figures, we use the eigenfunctions associated to points listed in Table 4. In addition, where conjugate points lead to different retinal images, we

Table 5

Conjugacy classes of symmetry-broken states represented by the point $V \in \mathbf{C}^6$, where $v = e^{i\pi/6}$. Scalar and pseudoscalar refer to states in [5]. $\Sigma_V \subset \Gamma$ is the isotropy group of the point V. ℓ denotes the number of conjugacy classes in Γ of each state.

| k	V	Comment	Σ_V	ℓ
0	$(1,1,1,1,1,1)$	scalar equilibrium	$\mathbf{D}_6(\kappa,\xi)$	1
	$(-1,-1,-1,-1,-1,-1)$	scalar equilibrium	$\mathbf{D}_6(\kappa,\xi)$	1
1	$(i,i,-v,\overline{v},\overline{v},-v)$	rotating wave	$\mathbf{D}_1(\kappa)$	6
	$(v^2,iv,-1,1,-iv,-v^2)$	rotating wave	$\mathbf{D}_1(\kappa\xi)$	6
2	$(1,1,-v^2,iv,iv,-v^2)$	equilibrium	$\mathbf{D}_2(\kappa,\xi^3)$	3
	$(-1,-1,v^2,-iv,-iv,v^2)$	equilibrium	$\mathbf{D}_2(\kappa,\xi^3)$	3
3	(i,i,i,i,i,i)	scalar equilibrium	$\mathbf{D}_3(\kappa,\xi^2)$	2
	$(1,-1,1,-1,1,-1)$	pseudoscalar equilibrium	$\mathbf{D}_3(\kappa\xi,\xi^2)$	2
4	$(1,1,iv,-v^2,-v^2,iv)$	equilibrium	$\mathbf{D}_2(\kappa,\xi^3)$	3
	$(-1,-1,-iv,v^2,v^2,-iv)$	equilibrium	$\mathbf{D}_2(\kappa,\xi^3)$	3
5	$(i,i,\overline{v},-v,-v,\overline{v})$	rotating wave	$\mathbf{D}_1(\kappa)$	6
	$(v^2,iv,-iv,-v^2,-1,1)$	rotating wave	$\mathbf{D}_1(\kappa\xi^5)$	6
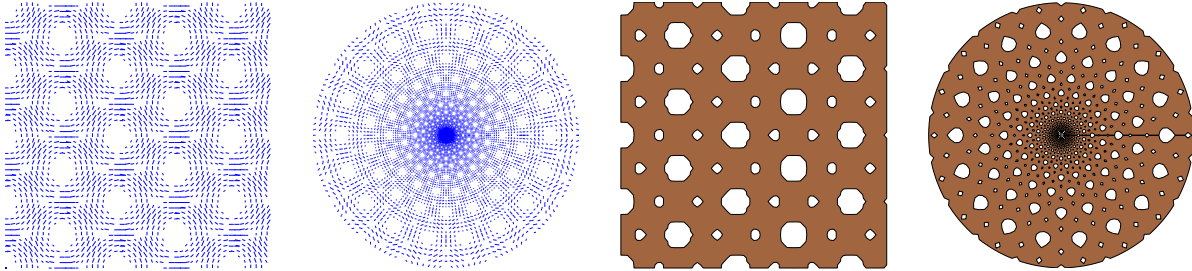
Figure 16. *Line field/thresholding of cortex/retinal images for planform $k = 0$.*

graph the planforms associated to these conjugate points. (In the figure captions, we indicate which group element produces the conjugacy.) Recall the discussion about retinal planforms and conjugate cortical planforms in section 1. Finally, we note that movies (time-periodic solutions) are associated to framed retinal images in Figures 17, 21, and 25–28.

3.4. The effects of weak anisotropy. Next we assume that the system is weakly anisotropic. That assumption is equivalent to assuming weak symmetry-breaking in the equations and generates more complicated dynamical descriptions corresponding to each maximal isotropy subgroup. We list these in turn.

3.4.1. The family $\Sigma_{k+1} = \mathbf{D}_6(\kappa, [0, 0, \frac{k\pi}{6}]\xi)$, $k = 0, \ldots, 5$. The results for these states are summarized in Table 5, and the details are found in section 4.8.1. See Figures 16–21.
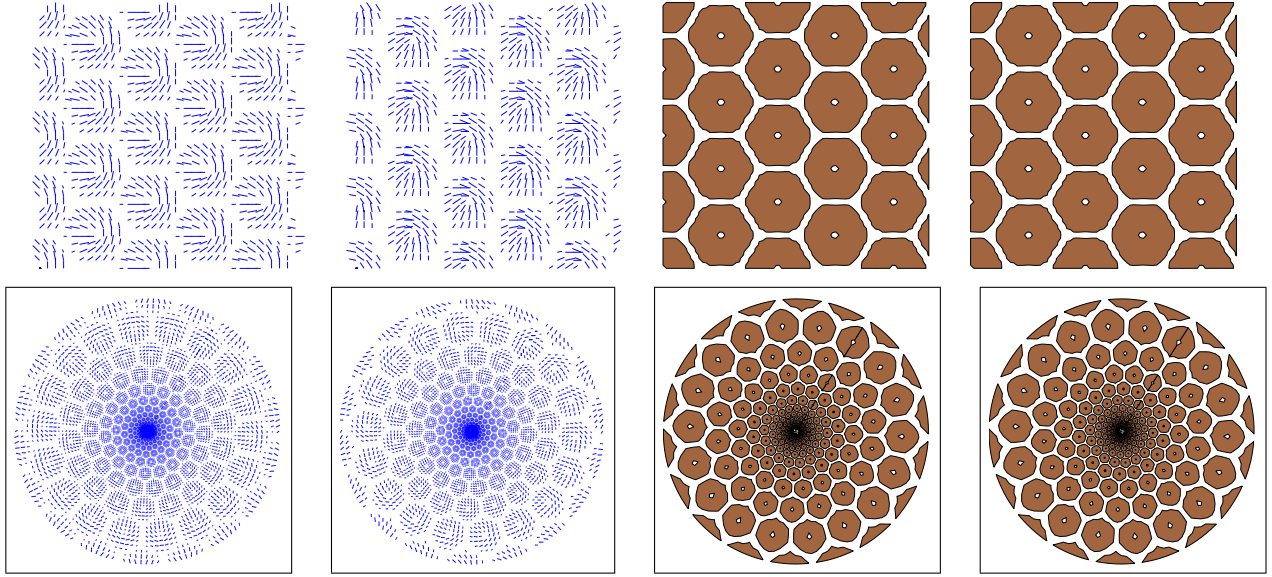
Figure 17. *Line field/thresholding of cortex/retinal images for planform $k = 1$. Second and fourth columns with ξ action; note that thresholded images with and without ξ action are identical. Movies are associated to framed images.*

3.4.2. $\Sigma_7 = \langle \kappa \xi^3, [0, \theta_2, 0], [\theta_1, 0, -\pi\theta_1] \rangle$. Steady states corresponding to Σ_7 persist as steady states under symmetry-breaking perturbations of the system and are conjugate to $T_1 = (1, 0, 0, 0, 0, 0)$. Details are found in section 4.8.2. Note that the eigenfunction for planform 7 is

$$\cos(2\phi + 2\pi \mathbf{k}_1 \cdot \mathbf{x}),$$

whose maximum value is 1 for every $\mathbf{x}$. It follows that sensible contouring cannot be obtained directly from the linear eigenfunction, and we present nonthresholded line field pictures in Figure 22. The same point is valid for the Σ_4 solutions on the square lattice.

3.4.3. $\Sigma_8 = \langle \kappa, \xi^3, [0, \theta_2, 0], [\frac{1}{2}, 0, \frac{\pi}{2}] \rangle$. In the anisotropic case, there are two conjugacy classes of equilibria corresponding to type Σ_8, namely, $(1, 1, 0, 0, 0, 0)$ and $(1, -1, 0, 0, 0, 0)$. These correspond to scalar and pseudoscalar rolls. Generically, there may be intermediate equilibria, and all dynamics on this group orbit converge to one of these equilibria. Details are found in section 4.8.3. See Figure 23.

3.4.4. $\Sigma_9 = \langle \xi^2, \kappa \xi, [\frac{1}{3}, \frac{1}{3}, \frac{2\pi}{3}] \rangle$. The dynamics on this group orbit is complicated to describe. We prove that there are at least two conjugacy classes of equilibria corresponding to $\pm(1, 0, 1, 0, 1, 0)$. Details are found in section 4.8.4. See Figure 24.
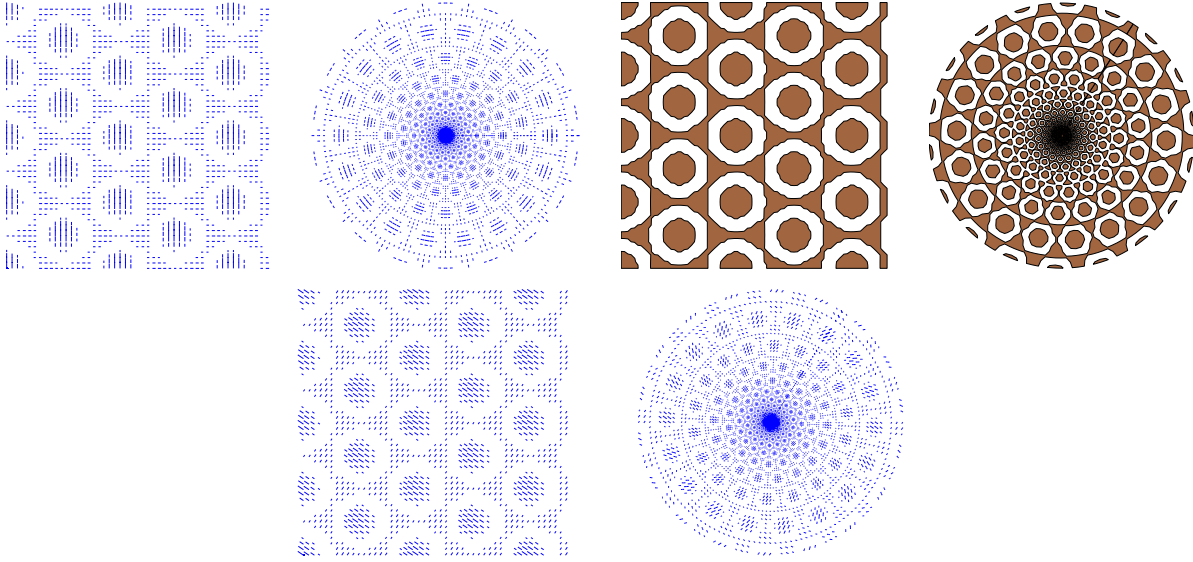
Figure 18. *Line field/thresholding of cortex/retinal images for planform $k = 2$. (Bottom) line fields with ξ action.*
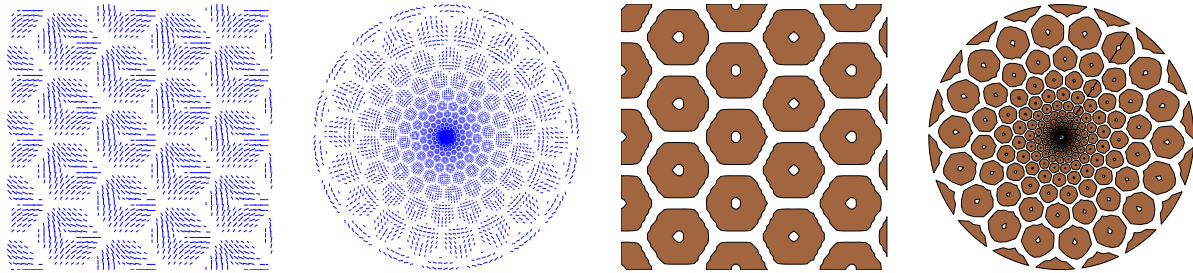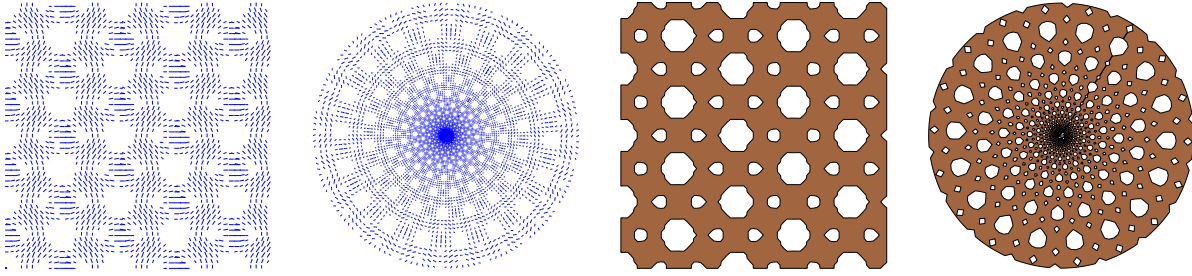

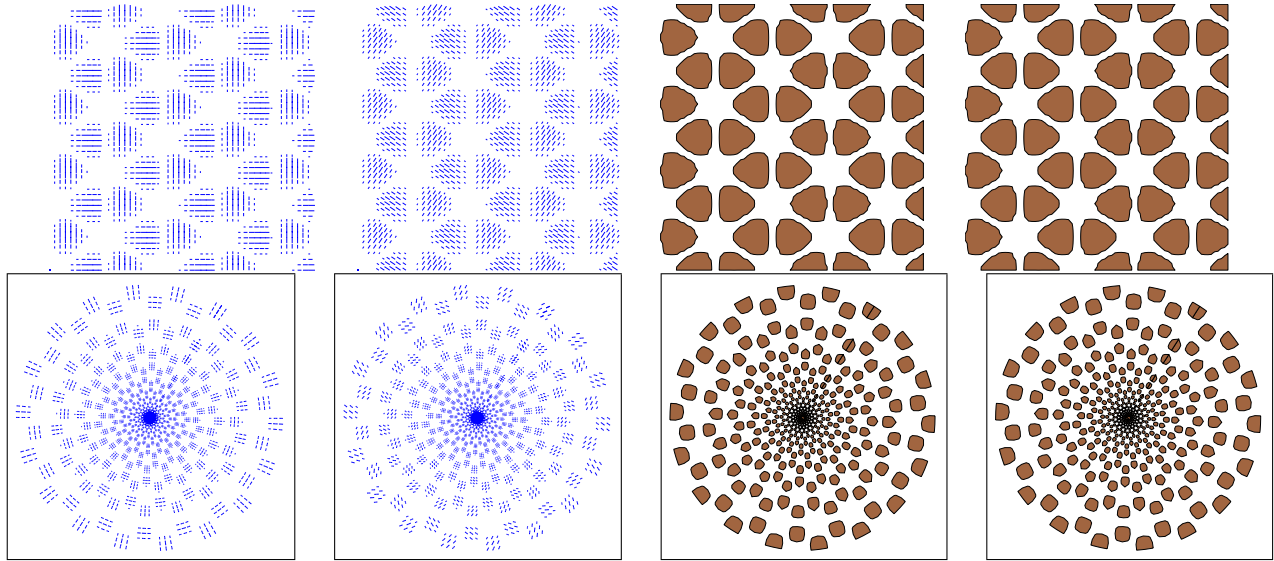**Figure 19.** *Line field/thresholding of cortex/retinal images for planform $k = 3$.*

3.4.5. $\Sigma_{10} = \langle \kappa\xi, [\theta_1, \theta_1, -\pi\theta_1] \rangle$. In the isotropic case, solutions corresponding to the maximal isotropy subgroup of type Σ_{10} can be expected to be a rotating wave, and the same is true in the anisotropic case. Up to conjugacy the rotating wave is $[\theta_1, -\theta_1, 0](1, 0, 1, 0, 0, 0)$. Details are found in section 4.8.5. See Figure 25.

3.4.6. $\Sigma_{11} = \langle \kappa\xi^4, [\theta_1, -\theta_1, -\pi\theta_1] \rangle$. In the isotropic case, solutions corresponding to the maximal isotropy subgroup of type Σ_{11} can be expected to be a rotating wave, and the same is true in the anisotropic case. Up to conjugacy the rotating wave is $[\theta_1, \theta_1, 0](1, 0, 0, 1, 0, 0)$. Details are found in section 4.8.6. See Figure 26.

3.4.7. $\Sigma_{12} = \langle \kappa\xi, \xi^3, [\frac{1}{2}, \frac{1}{2}, \frac{\pi}{2}] \rangle$. When symmetry breaks, equilibria and discrete rotating waves are possible. See Krauskopf [18, 19] and sections 4.7.3 and 4.8.7. See Figures 27 and 28 for possible equilibrium planforms.

Figure 20. *Line field/thresholding of cortex/retinal images for planform $k = 4$.*

Figure 21. *Line field/thresholding of cortex/retinal images for planform $k = 5$. Second and fourth columns with ξ action; note that thresholded images with and without ξ action are identical. Movies are associated to framed images.*

Note that in a system of PDEs (or in an integro-differential equation such as a Wilson–Cowan equation), a typical solution will be a function of both space and time. In such systems, a discrete rotating wave is a solution whose shape in space changes periodically in time; that is, the associated planform at different times need not be symmetry-related. The qualitative features of a movie of a discrete rotating wave are quite different from those of a (continuous) rotating wave.

4. Proofs of lattice results. In this section, we verify the results stated in sections 2 and 3.

Figure 22. *Line fields of cortex/retinal images for planform* 7. *(Second and fourth panels) line fields with* ξ *action. The maximum value of* $a(\mathbf{x}, \cdot)$ *is constant in* $\mathbf{x}$ *for these planforms, so thresholding is not relevant.*
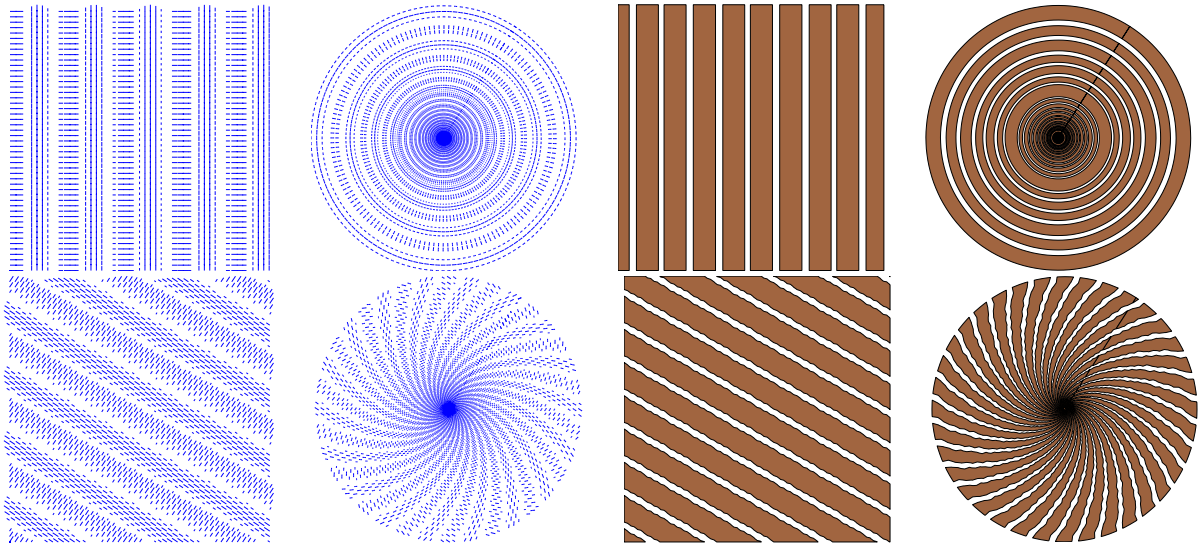
Figure 23. *Line field/thresholding of cortex/retinal images for planform* 8. *Bottom with* ξ *action.*

4.1. Verification of (2.1). Without loss of generality, we may assume that the planar square lattice $\mathcal{L}$ is the integer lattice and that the dual lattice $\mathcal{L}^*$ is generated by

$$\mathbf{k}_1 = (1,0) \quad \text{and} \quad \mathbf{k}_2 = (0,1).$$

Using Fourier series, we may write each function $f \in \mathcal{F}_{\mathcal{L}}$ as

$$f(\mathbf{x}, \phi) = \sum_{m,\mathbf{k}} z_{m,\mathbf{k}} e^{2im\phi} e^{2\pi i \mathbf{k} \cdot \mathbf{x}} + c.c.,$$

where $m \geq 0$, $\mathbf{k} \in \mathbf{Z}^2$, and $z_{m,\mathbf{k}} \in \mathbf{C}$. The functions corresponding to wave vectors of constant length k, namely,

$$V_k = \left\{ \sum_{m, |\mathbf{k}|=k} z_{m,\mathbf{k}} e^{2im\phi} e^{2\pi i \mathbf{k} \cdot \mathbf{x}} + c.c. \right\},$$
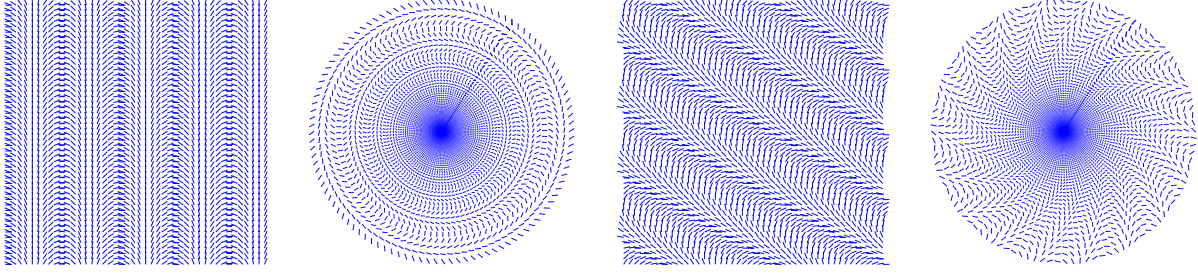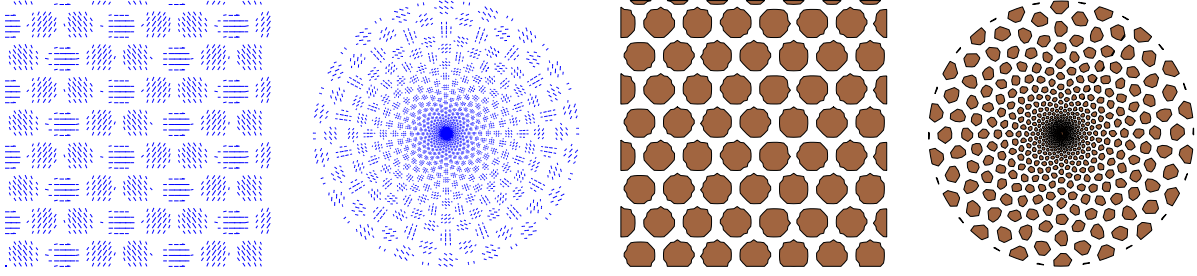
Figure 24. *Line field/thresholding of cortex/retinal images for planform* 9.
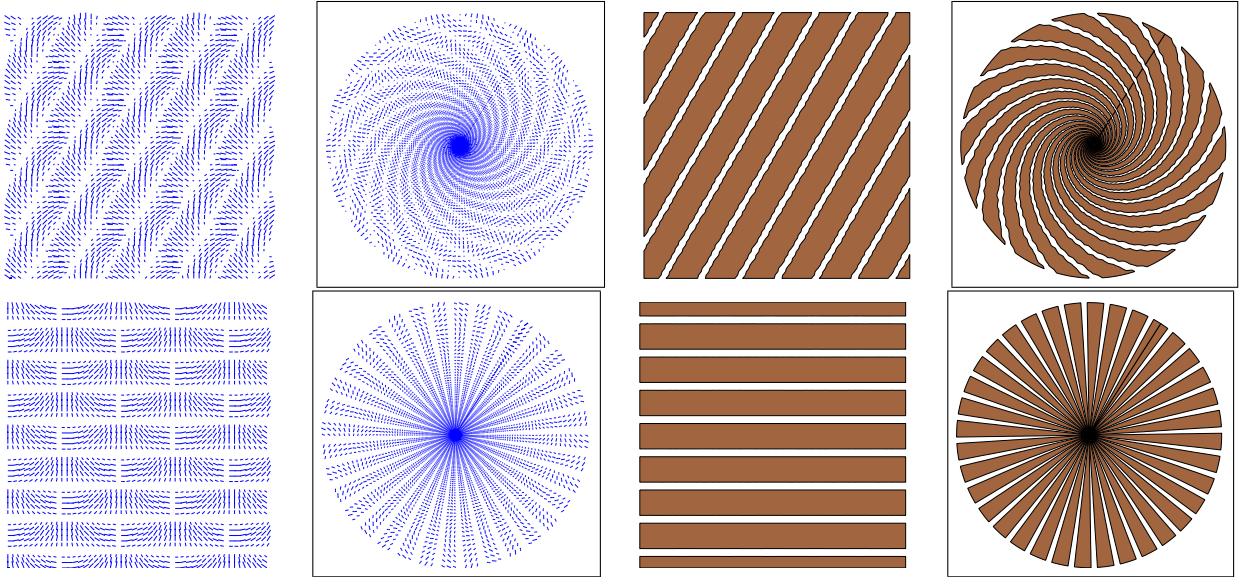
Figure 25. *Line field/thresholding of cortex/retinal images for planform* 10. *Bottom with ξ^2 action. Movies are associated to framed images.*

are $\widetilde{\Gamma}$-invariant subspaces. In this paper, we consider only steady-state bifurcations whose critical eigenspaces are irreducible subspaces in V_1, that is, those eigenfunctions corresponding to wave vectors of shortest length.

4.1.1. The irreducible subspaces of $V_1 \subset \mathcal{F}_\mathcal{L}$. The group $\widetilde{\Gamma}$ contains a 3-torus $\mathbf{T}^3$ generated by translations $\mathbf{y} \in \mathbf{T}^2$ and rotations $\widehat{\phi} \in \mathbf{S}^1$. For each $\mathbf{k} \in \mathcal{L}^*$ and $m \in \mathbf{Z}$, the two-dimensional subspaces

$$W_{\mathbf{k},m} = \{ze^{2im\phi}e^{2\pi i\mathbf{k}\cdot\mathbf{x}} + c.c. : \ z \in \mathbf{C}\} \subset \mathcal{F}_\mathcal{L}$$

are distinct irreducible representations of $\mathbf{T}^3$. Counterclockwise rotation ξ through angle $\pi/2$ and reflection κ across the horizontal axis generate $\widetilde{\Gamma}$ over $\mathbf{T}^3$, and

$$\theta W_{\mathbf{k},m} = W_{\theta\mathbf{k},m} \quad \text{and} \quad \kappa W_{\mathbf{k},m} = W_{\kappa\mathbf{k},-m}$$
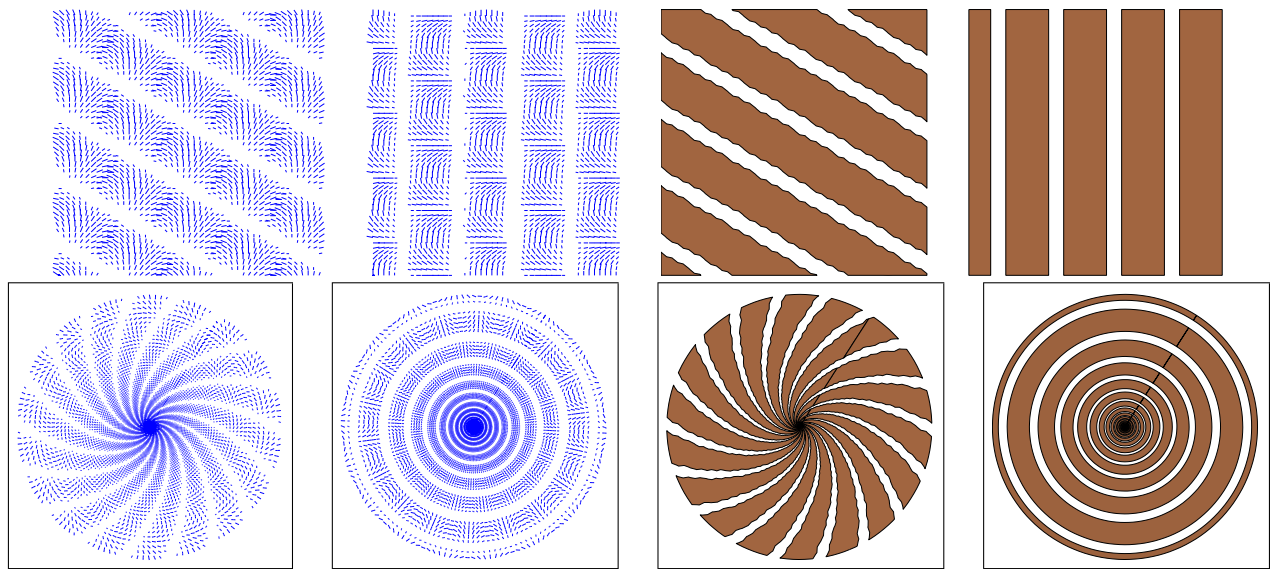
Figure 26. *Line field/thresholding of cortex/retinal images for planform* 11. *Second and fourth columns with ξ^2 action. Movies are associated to framed images.*
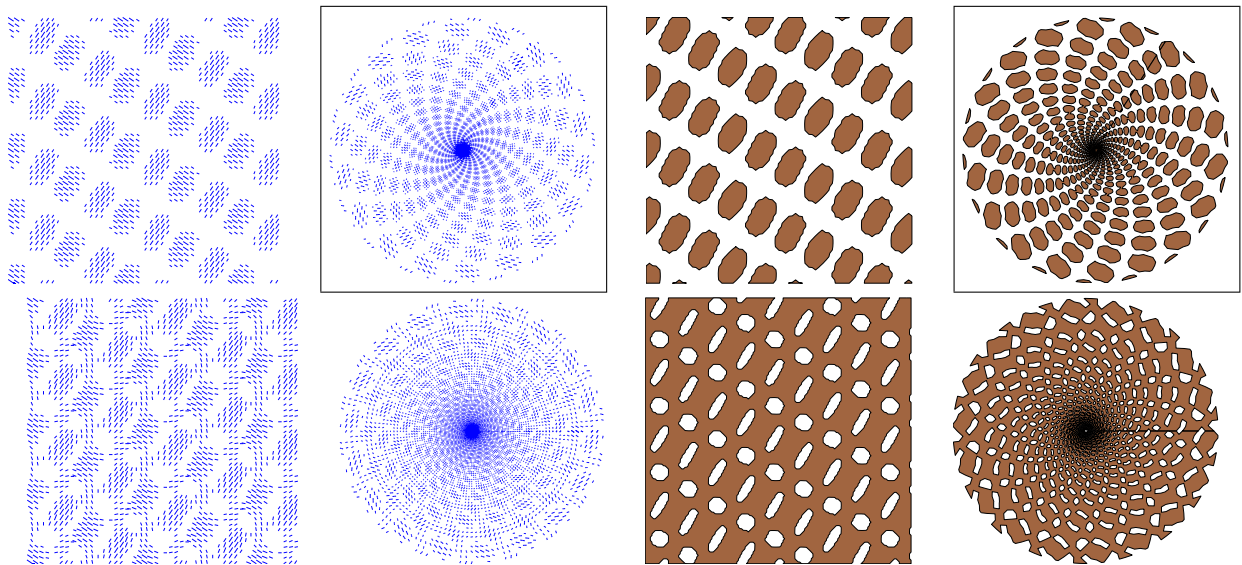
Figure 27. *Line field/thresholding of cortex/retinal images for planform 12: (Top) $u = 1$ and (bottom) $u = 0.5i$. Movies are associated to framed images.*

for any $\theta \in \mathbf{SO}(2)$. Finally,

$$W_{-\mathbf{k},-m} = W_{\mathbf{k},m}.$$
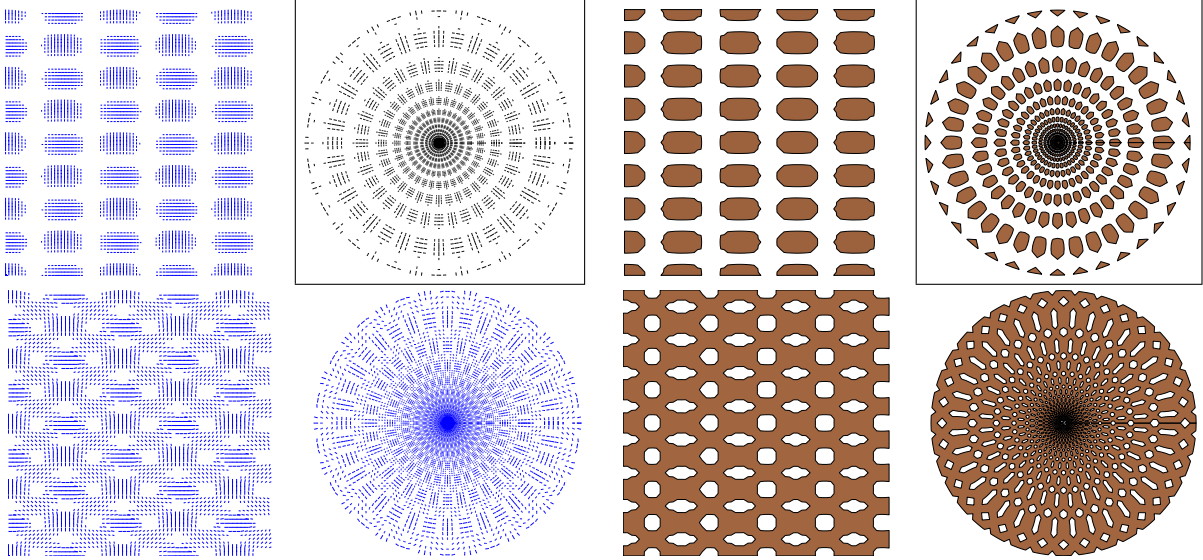
Figure 28. *Line field/thresholding of cortex/retinal images for planform* 12 *with* ξ^2 *action: (Top)* $u = 1$ *and (bottom)* $u = 0.5i$. *Movies are associated to framed images.*

Now fix $\mathbf{k} = \mathbf{k}_1$, and denote

$$W_m = \sum_{\gamma \in \mathbf{D}_4} \gamma W_{\mathbf{k}_1, m},$$

which is $\widetilde{\Gamma}$-invariant. The subspace W_0 is four-dimensional, and the subspaces W_m are eight-dimensional when $m > 0$. Indeed, W_m consists of all functions of the form (2.1). For $m > 0$, we identify $a(\mathbf{x}, \phi) \in W_m$ with $(z_1, w_1, z_2, w_2) \in \mathbf{C}^4$.

   Lemma 4.1. *The subspace* $W_m \subset \mathcal{F}_{\mathcal{L}}$ *is an absolutely irreducible representation of* $\widetilde{\Gamma}$.

   Proof. The case in which $m = 0$ is established by Lemma 3.1 in [5]. For $m > 0$, write $W_m = W_m^+ \oplus W_m^-$ as a sum of even and odd functions of ϕ (that is, $\cos(2m\phi)$ and $\sin(2m\phi)$). The summands are absolutely irreducible and nonisomorphic (look at the action of κ) for $\mathbf{D}_4 \dot{+} \mathbf{T}^2$ by Lemma 3.1 in [5]. Thus any matrix commuting with $\widetilde{\Gamma}_{\mathcal{L}}$ on W_m is block diagonal, with each diagonal block being a real multiple of the identity. Now the extra $\mathbf{S}^1$-symmetry forces the two diagonal blocks to be equal. (Consider specifically $[0, 0, \frac{\pi}{4}]$, which interchanges W_m^+ and W_m^-.)   ∎

   4.2. Group action and isotropy subgroups. Fix $m > 0$. The action of $\widetilde{\Gamma}$ is given in Table 6, where we denote elements in the 2-torus $\mathbf{T}^2$ of translations by $[\theta_1, \theta_2]$. Recall that $0 \leq \theta_j < 1$, since the lattice is 1-periodic, $\widehat{\phi}$ is π-periodic, and $a \in W_m$ given by (2.1) is identified with $(z_1, w_1, z_2, w_2) \in \mathbf{C}^4$.

Table 6

Group action on $(z_1, w_1, z_2, w_2) \in W_m = \mathbf{C}^4$; $\xi, \kappa \in \mathbf{D}_4$, $0 \le \theta_1, \theta_2 < 1$, *and* $0 \le \widehat{\phi} < \pi$.

Generators	Action
ξ	$(\overline{w}_2, \overline{z}_2, z_1, w_1)$
κ	$(w_1, z_1, \overline{z}_2, \overline{w}_2)$
$[\theta_1, \theta_2, 0]$	$(e^{2\pi i \theta_1} z_1, e^{2\pi i \theta_1} w_1, e^{2\pi i \theta_2} z_2, e^{2\pi i \theta_2} w_2)$
$[0, 0, \widehat{\phi}]$	$(e^{-2im\widehat{\phi}} z_1, e^{2im\widehat{\phi}} w_1, e^{-2im\widehat{\phi}} z_2, e^{2im\widehat{\phi}} w_2)$

Table 7

$u, v \in \mathbf{C}$, $a, b \in \mathbf{R}$.

	Normal form	Generators	Fixed subspace	Dim
0	$(0,0,0,0)$	$\widetilde{\Gamma}$	0	0
1	$(1,1,1,1)$	κ, ξ	$\mathbf{R}\{(1,1,1,1)\}$	1
2	$(1,1,1,-1)$	$\kappa, \left[\frac{3}{4}, \frac{1}{4}, \frac{\pi}{4}\right] \xi$	$\mathbf{R}\{1,1,1,-1\}$	1
3	$(1,1,0,0)$	$\kappa, \xi^2, [0,\theta_2,0]$	$\mathbf{R}\{(1,1,0,0)\}$	1
4	$(1,0,0,0)$	$\kappa\xi^2, [0,\theta_2,0], [\theta_1,0,\pi\theta_1]$	$\mathbf{R}\{(1,0,0,0)\}$	1
5	$(1,0,1,0)$	$\kappa\xi, [\theta_1,\theta_1,\pi\theta_1]$	$\{(u,0,\overline{u},0\}$	2
6	$(1,1,b,b)$	κ, ξ^2	$\{(a,a,b,b)\}$	2
7	$(1,1,-b,b)$	$\kappa, \left[0, \frac{1}{2}, 0\right] \xi^2$	$\{(a,a,-b,b)\}$	2
8	$(i,-i,-i,i)$	$\kappa\xi, \xi^2$	$\{(u,\overline{u},\overline{u},u)\}$	2
9	$(1,b,0,0)$	$\kappa\xi^2, [0,\theta_2,0]$	$\{(a,b,0,0)\}$	2
10	$(1,1,b,b)$	ξ^2	$\{(u,\overline{u},v,\overline{v})\}$	4
11	$(1,1,a,b)$	κ	$\{(u,u,a,b)\}$	4
12	$(1,b,1,b)$	$\kappa\xi$	$\{(u,v,\overline{u},\overline{v})\}$	4
13	$(1,0,b,0)$	$[\theta_1,\theta_1,\pi\theta_1]$	$\{(u,0,v,0)\}$	4
14		1	$\mathbf{C}^4$	8

Note that the action always has a nontrivial kernel $\mathbf{Z}_{4m}$ generated by the element

$$\left[\theta_1, \theta_2, \widehat{\phi}\right] = \left[\frac{1}{2}, \frac{1}{2}, \frac{\pi}{2m}\right].$$

In order to simplify the presentation, we will not include this kernel explicitly in the isotropy subgroups. Indeed, the bifurcation analysis is identical for all $m \ge 1$. (Just factor out the kernel.) The case in which $m = 0$ was considered in [5]. Hence, without loss of generality, we assume that $m = 1$. The assumption that $m = 1$ does make a difference in the planforms— but in a very controllable way. The case in which $m \ge 2$ differs from $m = 1$ by the fact that the activity function $a(\mathbf{x}, \cdot)$ restricted to the unit circle at $\mathbf{x}$ has period π/m instead of π. Therefore, the maxima of this activity variable occur simultaneously at m points on that circle rather than at a single point.

Using the group action given in Table 6, we can compute the lattice of isotropy subgroups

(up to conjugacy) of the action of $\widetilde{\Gamma}$ on W_1. The results for $m = 1$ are given in Table 7.

We verify that up to conjugacy the maximal subgroups are those shown in Table 7. Let $z = (z_1, w_1, z_2, w_2)$. Our strategy is based on the fact that conjugate points have conjugate isotropy subgroups. Moreover, it is convenient to note that multiplying z by a nonzero real number does not change its isotropy subgroup. So we can conjugate z by elements of $\widetilde{\Gamma}$ and scale z to put z into a "normal form." Once we have the normal form, we compute generators for the isotropy subgroups of that normal form.

There is a useful remark that concerns conjugating z with 3-torus $\mathbf{T}^3 = \{[\theta_1, \theta_2, \widehat{\phi}]\}$ elements: z can be conjugated by an element in $\mathbf{T}^3$ so that any three of its nonzero coordinates are real and positive.

We discuss only maximal isotropy subgroups: cases **0** to **5**. First, we classify the isotropy subgroups of z when z has some of its coordinates equal to zero. If $z = 0$, then its isotropy subgroup is $\widetilde{\Gamma}$, which is case **0**. If three of the coordinates of z are zero, then z is conjugate to $(1, 0, 0, 0)$, and we have case **4**. If two of the coordinates of z are zero, then we can assume after conjugacy that the other two coordinates are real and positive. After conjugacy, by elements in $\mathbf{D}_4$ we can assume that the fourth coordinate and either the second or the third coordinate is zero. Thus, after scaling, z has the normal form $(1, 0, b, 0)$ or $(1, b, 0, 0)$, where $b \geq 1$. If $b = 1$, then we have cases **5** and **3**. (If $b > 1$, then we have cases **13** and **9**, which are not maximal.)

Next, we assume that all coordinates of z are equal in modulus. After scaling, we assume that all coordinates have modulus one, and after conjugating by an element in $\mathbf{T}^3$ we can assume that $z = (1, 1, 1, e^{2\pi i \rho})$. Observe that $\kappa z = (1, 1, 1, e^{-2\pi i \rho})$. After conjugacy, it follows that we may assume $0 \leq \rho \leq \frac{1}{2}$. We consider three possibilities: $\rho = 0$, $\rho = \frac{1}{2}$, and $0 < \rho < \frac{1}{2}$. Note that $\rho = 0$ is $z = (1, 1, 1, 1)$, which is case **1**. When $\rho = \frac{1}{2}$, then $z = (1, 1, 1, -1)$; the isotropy subgroup is $\langle \kappa, [\frac{3}{4}, \frac{1}{4}, \frac{\pi}{4}]\xi \rangle \cong \mathbf{D}_4$, which is case **2**. Finally, when $0 < \rho < \frac{1}{2}$; the isotropy subgroup is $\langle [0, \rho, 0]\xi^2, [\frac{\rho}{2}, \frac{\rho}{2}, \frac{\pi \rho}{2}]\kappa\xi \rangle$, which is conjugate to $\langle \kappa\xi, \xi^2 \rangle$ by $[0, -\frac{\rho}{2}, -\frac{\pi \rho}{4}]$. This is case **8**, which is not maximal.

Finally, all z whose coordinates are nonzero and not of equal modulus have isotropy subgroups that are not maximal.

4.3. Equivariants of $\widetilde{\Gamma}$ acting on W_1 in square lattice. Let $F : \mathbf{C}^4 \to \mathbf{C}^4$ be a $\widetilde{\Gamma}$-equivariant polynomial mapping. We can write the form of F in terms of invariant generators using standard invariant theory, and we do so in Theorem 4.1. The proof of this theorem uses standard techniques and is not presented here. For background, see [14].

In complex coordinates, we can write F as

(4.1) $$F = (Z_1, W_1, Z_2, W_2).$$

Using the $\mathbf{D}_4$-equivariance of F (specifically $\kappa, \xi^3, \kappa\xi^3$), we see that

$$(4.2) \qquad \begin{aligned} W_1(z_1, w_1, z_2, w_2) &= Z_1(w_1, z_1, \overline{z}_2, \overline{w}_2), \\ Z_2(z_1, w_1, z_2, w_2) &= Z_1(z_2, w_2, \overline{w}_1, \overline{z}_1), \\ W_2(z_1, w_1, z_2, w_2) &= Z_1(w_2, z_2, w_1, z_1). \end{aligned}$$

In addition, Z_1 must satisfy $\mathbf{T}^3$-invariance conditions

$$(4.3) \qquad Z_1(e^{2\pi i\theta_1} z_1, e^{2\pi i\theta_1} w_1, z_2, w_2) = e^{2\pi i\theta_1} Z_1(z_1, w_1, z_2, w_2),$$

$$(4.4) \qquad Z_1(z_1, w_1, e^{2\pi i\theta_2} z_2, e^{2\pi i\theta_2} w_2) = Z_1(z_1, w_1, z_2, w_2),$$

$$(4.5) \qquad Z_1(z_1, e^{2\pi i\widehat{\phi}} w_1, z_2, e^{2\pi i\widehat{\phi}} w_2) = Z_1(z_1, w_1, z_2, w_2)$$

as well as

$$(4.6) \qquad Z_1(\overline{z}_1, \overline{w}_1, w_2, z_2) = \overline{Z_1(z_1, w_1, z_2, w_2)}.$$

Here we take as $\mathbf{T}^3$ generators the circles $(\theta_1, 0, 0)$, $(0, \theta_2, 0)$, and $(\widehat{\phi}/2, \widehat{\phi}/2, \pi\widehat{\phi}/2)$.

$\quad$ *Theorem* 4.1. *The invariance conditions* (4.3)–(4.5) *and* (4.6) *imply that the polynomial* Z_1 *has the form*

$$\begin{aligned} Z_1 = {} & C(|z_1|^2, |w_1|^2, |z_2|^2 + |w_2|^2, i(|z_2|^2 - |w_2|^2), z_1\overline{w}_1\overline{z}_2 w_2)z_1 \\ & + D(|z_1|^2, |w_1|^2, |z_2|^2 + |w_2|^2, i(|z_2|^2 - |w_2|^2), \overline{z}_1 w_1 z_2 \overline{w}_2)w_1 z_2 \overline{w}_2, \end{aligned}$$

where C and D are polynomials with real coefficients. Moreover, this form is unique.

4.4. Existence of time-periodic rotating waves. We claim that generically there is a branch of time-periodic rotating wave solutions corresponding to the maximal isotropy subgroup Σ_5; moreover, the period of these solutions tends to infinity at the bifurcation point. To verify these statements, we must use the $\widetilde{\Gamma}$-equivariant polynomials on $\mathbf{C}^4$.

$\quad$ We assume that (4.1), with bifurcation parameter λ, is obtained by a center manifold reduction so that the asymptotic dynamics of the differential equation is reproduced by (4.1). Observe that (4.1) restricted to $\mathrm{Fix}(\Sigma_5)$ is given by

$$(4.7) \qquad \begin{aligned} \frac{du}{dt} &= Z_1(u, 0, \overline{u}, 0, \lambda) \\ &= C(|u|^2, 0, |u|^2, i|u|^2, 0, \lambda)u \\ &= \left(c_\lambda \lambda + (c_1 + c_3)|u|^2 + c_4 i|u|^2 + \cdots\right)u, \end{aligned}$$

where

$$(4.8) \qquad C = c_1|z_1|^2 + c_2|w_1|^2 + c_3(|z_2|^2 + |w_2|^2) + c_4 i(|z_2|^2 - |w_2|^2) + c_\lambda \lambda + \cdots$$

and $c_1, c_2, c_3, c_4, c_\lambda$ are real constants. Write $u = \rho e^{i\tau}$ in polar coordinates, and write (4.7) as phase amplitude equations (to third order) obtaining

$$\frac{d\rho}{dt} = (c_\lambda \lambda + (c_1 + c_3)\rho^2)\rho,$$
$$\frac{d\tau}{dt} = c_4 \rho^2.$$

Assume that the *eigenvalue crossing condition*

(4.9) $$c_\lambda \neq 0$$

is valid. Then there exists an invariant circle for the dynamics (given by a zero to the amplitude equation) at

$$\lambda = -\frac{c_1 + c_3}{c_\lambda}\rho^2,$$

and the invariant is a periodic solution if the nondegeneracy condition

$$c_4 \neq 0$$

holds. Note that the frequency of the periodic solution is $c_4\rho^2/2\pi$, which goes to zero at the bifurcation point.

4.5. Stability of maximal isotropy solutions. The following computations were done using Mathematica for the equivariant F determined by Theorem 4.1, where

$$C(|z_1|^2, |w_1|^2, |z_2|^2 + |w_2|^2, i(|z_2|^2 - |w_2|^2), z_1\overline{w}_1\overline{z}_2 w_2, \lambda)$$
(4.10)
$$= c_1|z_1|^2 + c_2|w_1|^2 + c_3(|z_2|^2 + |w_2|^2) + c_4 i(|z_2|^2 - |w_2|^2) + c_\lambda \lambda + \cdots$$
$$D(|z_1|^2, |w_1|^2, |z_2|^2 + |w_2|^2, i(|z_2|^2 - |w_2|^2), \overline{z}_1 w_1 z_2 \overline{w}_2, \lambda)$$
$$= d_0 + d_\lambda \lambda + \cdots.$$

Table 8 describes necessary and sufficient conditions for the orbital asymptotic stability of $\widetilde{\Gamma}$-orbits of fixed points and periodic orbits corresponding to the maximal isotropy subgroups of the action on the square lattice near bifurcation. This stability refers to perturbations in the class of spatially periodic functions on the square lattice. These conditions were obtained by computing the eigenvalues of the differential of a $\widetilde{\Gamma}$-equivariant vector field (to lowest order in the bifurcation parameter) and requiring that those eigenvalues that are not forced to be zero by symmetry have negative real part.

Table 8

Stability of maximal isotropy types for the square lattice; $dZ/dt = F(Z, \lambda)$, with F determined by (4.10). *Numbering of isotropy groups is as in Table* 7.

Group	Solution	Stability conditions				
1	equilibrium	$c_1 - c_2 - d_0 < 0$	$c_1 + c_2 \pm (2c_3 + d_0) < 0$	$d_0 > 0$		
2	equilibrium	$c_1 - c_2 + d_0 < 0$	$c_1 + c_2 \pm (2c_3 - d_0) < 0$	$d_0 < 0$		
3	equilibrium	$c_1 \pm c_2 < 0$	$-c_1 - c_2 + 2c_3 \pm d_0 < 0$			
4	equilibrium	$c_2 - c_1 < 0$	$c_3 - c_1 < 0$	$c_1 < 0$		
5	periodic	$c_2 - c_1 \pm d_0 < 0$	$c_1 \pm c_3 < 0$		$c_\lambda > 0$	$c_4 \neq 0$

4.6. Effect of weak anisotropy on square lattice. The study of forced symmetry-breaking requires the following general result.

Lemma 4.2. *Let $K \subset H$ be compact subgroups in $\mathbf{O}(n)$. Assume that the H-equivariant vector field $F : \mathbf{R}^n \to \mathbf{R}^n$ has a normally hyperbolic, flow-invariant, H-invariant compact manifold S contained in $\mathrm{Fix}(K)$. Let $F' : \mathbf{R}^n \to \mathbf{R}^n$ be a small H-equivariant perturbation of F.*

Then F' has a unique flow-invariant manifold S' near S that is also H-invariant, contained in $\mathrm{Fix}(K)$, diffeomorphic to S, and normally hyperbolic for F'.

Proof. Normal hyperbolicity implies that any small perturbation of F (equivariant or not) will have a unique flow-invariant set S' that is close to (and diffeomorphic to) S. (See Hirsch, Pugh, and Shub [15].)

Since the subspace $\mathrm{Fix}(K)$ is preserved by all H-equivariant vector fields, we can apply the previous result to the vector fields restricted to $\mathrm{Fix}(K)$ and conclude that there is an F'-invariant set $S'' \subset \mathrm{Fix}(K)$ near S. Uniqueness forces $S' = S''$. Similarly, uniqueness forces S' to be H-invariant. Let $h \in H$. Then $h(S')$ is also F'-invariant and close to S (because $h(S) = S$); hence $h(S')$ must coincide with S'. ∎

4.6.1. Squares: $\Sigma_1 = \mathbf{D}_4(\kappa, \xi)$. Let $S_1 = (1, 1, 1, 1)$. The isotropy subgroup Σ_1 of S_1 is axial, with fixed-point subspace $V_0 = \mathbf{R}\{S_1\}$. The Equivariant Branching Lemma implies that a generic $\widetilde{\Gamma}$ bifurcation with kernel W_1 has a branch of solutions $Z(\lambda) = u(\lambda)S_1$, $u(\lambda) > 0$, in V_0 with symmetry Σ_1. When discussing forced symmetry-breaking of this equilibrium, which we assume to be normally hyperbolic, we can assume that $u(\lambda) = 1$.

The equilibria that are conjugate by a $\widetilde{\Gamma}$-symmetry to S_1 fill out the 3-torus

$$\mathbf{T}^3 = \{(z_1, w_1, z_2, w_2) : |z_1| = |w_1| = |z_2| = |w_2|, z_1 \overline{w}_1 \overline{z}_2 w_2 = 1\},$$

and each point on $\mathbf{T}^3$ has the form $[\theta_1, \theta_2, \widehat{\phi}]S_1$. Recall that the isotropy subgroup of σv is

$\Sigma_{\sigma v} = \sigma \Sigma_v \sigma^{-1}$. A short calculation shows that

$$[\theta_1, \theta_2, \widehat{\phi}]\xi = \xi[\theta_2, -\theta_1, \widehat{\phi}],$$
$$[\theta_1, \theta_2, \widehat{\phi}]\kappa = \kappa[\theta_1, -\theta_2, -\widehat{\phi}].$$

It follows that

$$[\theta_1, \theta_2, \widehat{\phi}]\xi[-\theta_1, -\theta_2, -\widehat{\phi}] = \xi[\theta_2 - \theta_1, -\theta_2 - \theta_1, 0],$$
$$[\theta_1, \theta_2, \widehat{\phi}]\kappa[-\theta_1, -\theta_2, -\widehat{\phi}] = \kappa[0, -2\theta_2, -2\widehat{\phi}].$$

Thus, when symmetry breaks from $\widetilde{\Gamma}$ to Γ, the isotropy subgroup of $[\theta_1, \theta_2, \widehat{\phi}]S_1$ is isomorphic to $\mathbf{Z}_4(\xi)$ unless $\widehat{\phi} = 0, \frac{\pi}{4}, \frac{\pi}{2}, \frac{3\pi}{4}$. The reason that $\widehat{\phi} = \pm\frac{\pi}{4}$ are possibilities is that $[\frac{1}{2}, \frac{1}{2}, \frac{\pi}{2}]$ is in the kernel of $\widetilde{\Gamma}$ acting on $\mathbf{C}^4$. In these exceptional cases, the isotropy subgroup of $[\theta_1, \theta_2, \widehat{\phi}]S_1$ is isomorphic to $\mathbf{D}_4(\kappa, \xi)$.

Since $\dim \mathrm{Fix}(\mathbf{D}_4) = 1$, it follows from Lemma 4.2 that both S_1 and

$$S_2 \equiv \left[\frac{1}{4}, \frac{1}{4}, \frac{\pi}{4}\right] S_1 = (1, -1, 1, -1)$$

remain as equilibria when small anisotropy is assumed. Points conjugate to S_1 in Γ are scalar squares (Esquares in [5]), and points conjugate to S_2 in Γ are pseudoscalar squares (Osquares in [5]).

The fixed-point subspace of $\mathbf{Z}_4(\xi)$ is two-dimensional and consists of vectors of the form $(u, \overline{u}, u, \overline{u})$. The intersection of this fixed-point subspace with the torus $\mathbf{T}^3$ is the circle where $|u| = 1$. It follows by conjugacy that the flow of the vector field restricted to $\mathbf{T}^3$ when the isotropy subgroup is conjugate to $\mathbf{Z}_4$ is on circles. Moreover, each circle has four equilibria, points conjugate to $\pm S_1$ in Γ and points conjugate to $\pm S_2$. Depending on the exact form of the anisotropy in model equations, it is possible for there to be additional equilibria on these circles.

4.6.2. $\Sigma_2 = \mathbf{D}_4(\kappa, [\frac{3}{4}, \frac{1}{4}, \frac{\pi}{4}]\xi)$. The verification that forced symmetry-breaking leads to equilibria in this case is similar in spirit to that for Σ_1 in section 4.6.1, although the details are somewhat different. We can show that all points on the $\widetilde{\Gamma}$ group orbit 3-torus of equilibria have isotropy subgroup in Γ containing a group element conjugate to ξ^2. This fact forces the Γ-equivariant dynamics on the torus to be constrained to circles given by the action of $\widehat{\phi}$. Moreover, on each of these circles, there are eight points whose Γ isotropy subgroup contains group elements conjugate to κ or $\kappa\xi$. These points are forced to remain as equilibria for Γ-equivariant perturbations. Thus, as in the Σ_1 case, the trajectories of the forced symmetry-broken flow converge to equilibria.

4.6.3. Rolls: $\Sigma_3 = \langle \kappa, \xi^2, [0, \theta_2, 0] \rangle$. The analysis of Σ_3 steady states is similar to that done in section 4.6.1 for Σ_1; therefore, we just sketch the details.

Let $R_1 = (1, 1, 0, 0)$. The isotropy subgroup Σ_3 is axial, with fixed-point space $V_0 = \mathbf{R}\{R_1\}$; hence generically a branch of steady states $Z(\lambda) = u(\lambda)(1, 1, 0, 0)$ exists. Again, when discussing forced symmetry-breaking, we may assume that $u(\lambda) = 1$.

The steady states conjugate to R_1 in $\widetilde{\Gamma}$ form two 2-tori that are conjugate by ξ. Since this symmetry is not lost when we break symmetry from $\widetilde{\Gamma}$ to Γ, it is enough to analyze one of these tori. We focus on the torus given by the orbit of R_1 under $[\theta_1, 0, \widehat{\phi}]$, the connected component of $\widetilde{\Gamma}$. This torus is contained in $\mathrm{Fix}([0, \theta_2, 0])$ and has the form

$$\mathbf{T}^2 = \{(z_1, w_1, 0, 0) : |z_1| = |w_1| = 1\}.$$

The isotropy subgroups of these points are conjugate to either Σ_3 or the index two subgroup $\langle \xi^2, [0, \theta_2, 0] \rangle$. The former leads to equilibria and the latter to flow-invariant circles on $\mathbf{T}^2$. The equilibria are conjugate either to R_1 (scalar rolls) or to $R_2 = (1, -1, 0, 0)$ (pseudoscalar rolls).

As before, each circle has at least four equilibria, points conjugate in Γ to $\pm R_1$ and $\pm R_2$. Depending on the exact form of the anisotropy in model equations, it is possible for there to be additional equilibria on these circles.

4.6.4. $\Sigma_4 = \langle \kappa \xi^2, [0, \theta_2, 0], [\theta_1, 0, \pi \theta_1] \rangle$. We claim that steady states corresponding to Σ_4 persist as steady states under symmetry-breaking perturbations of the system. Let $T_1 = (1, 0, 0, 0)$. The isotropy subgroup Σ_4 of T_1 is axial and, by the Equivariant Branching Lemma, leads generically to a branch of steady states $Z(\lambda) = u(\lambda)T_1$ with symmetry Σ_4.

The connected group orbit through T_1 is the circle $[\theta_1, 0, 0]T_1$. Since

$$\mathrm{Fix}(\langle \kappa \xi^2, [0, \theta_2, 0] \rangle) = \{(a, b, 0, 0) : a, b \in \mathbf{R}\}$$

intersects the circle in two points, these points are equilibria. Since points on this circle are conjugate in Γ, it follows that all points on the circle are equilibria. There are three conjugate circles of steady states obtained by applying κ, ξ, and $\xi\kappa$.

4.6.5. Rotating spirals: $\Sigma_5 = \langle \kappa\xi, [\theta_1, \theta_1, \pi\theta_1] \rangle$. In subsection 4.4, we showed that generically a branch of time-periodic rotating waves bifurcates in the fixed-point subspace of isotropy subgroup Σ_5. We show that these rotating waves persist when symmetry is broken to Γ.

Note that the connected group orbit that contains the rotating waves is the 2-torus $[\theta_1, \theta_2, 0](1, 0, 1, 0)$. Since the fixed-point subspace of $\kappa\xi$ intersects the torus in a circle, it follows that the flow on this torus is restricted to circles. Finally, the fact that $[\theta_1, -\theta_1, 0]$

normalizes the isotropy subgroup of $(1,0,1,0)$ forces the flow on the circles to be a rotating wave. Since these statements rely only on elements in Γ, it follows that the solutions remain rotating waves even after a symmetry-breaking perturbation.

4.7. Maximal isotropy groups for the hexagonal lattice. In this section, we will find maximal isotropy groups for the hexagonal lattice action. Namely, we will describe vectors $Z = (z_1, w_1, z_2, w_2, z_3, w_3) \in \mathbf{C}^6$ such that Σ_Z is a maximal isotropy group.

We will look at the cases determined by the number of nonzero elements of Z. Since we are interested only in the maximal isotropy groups, the following lemma is useful.

Lemma 4.3. *If Σ_Z is a maximal isotropy group, then there is a vector Z' such that $\Sigma_Z = \Sigma_{Z'}$ and all nonzero entries of Z' have the same absolute value.*

Proof. Denote $\ell = \max\{|z_i|, |w_i|\} > 0$, and let Z' be the element obtained from Z by setting to zero all entries whose absolute value is not equal to ℓ. Then, each element $\sigma \in \widetilde{\Gamma}$ that fixes Z fixes Z' as well (since the action of $\widetilde{\Gamma}$ at most permutes the set of absolute values of the entries of Z; see Table 3); that is, $\Sigma_Z \subset \Sigma_{Z'}$. If Σ_Z is maximal, then the inclusion has to be equality. ∎

Denote by $N(Z)$ the number of nonzero entries of Z. By the previous lemma, we can assume that each nonzero element has absolute value equal to 1. Notice that the action of $\mathbf{D}_6$ either preserves the z_i- and w_i-positions or interchanges them. Moreover, the pairs (z_i, w_i) are never "broken up."

By the notation $t\sigma$ for an element of $\widetilde{\Gamma}$, we mean that $t = [\theta_1, \theta_2, \widehat{\phi}] \in \mathbf{T}^3$ and $\sigma \in \mathbf{D}_6$. We use the numbering of isotropy groups given in Table 4.

$\mathbf{N(Z)} = \mathbf{1}$. Use $\mathbf{D}_6$ to make $z_1 \neq 0$, and then apply θ_1 to obtain $z_1 > 0$. This gives case **7**.

$\mathbf{N(Z)} = \mathbf{2}$. Up to the action of $\mathbf{D}_6$, there are three possibilities for the position of the nonzero elements. We then use $\mathbf{T}^3$ to make the entries positive (hence equal):

(a) $Z = (1, 1, 0, 0, 0, 0)$ is case **8**.

(b) $Z = (1, 0, 1, 0, 0, 0)$ is case **10**.

(c) $Z = (1, 0, 0, 1, 0, 0)$ is case **11**.

$\mathbf{N(Z)} = \mathbf{3}$. Again, we use the action of $\mathbf{D}_6$ to bring the nonzero elements to the "leftmost" positions, followed by $\mathbf{T}^3$ to make them positive (hence equal). There are four cases:

(a) $Z = (1, 0, 1, 0, 1, 0)$ is case **9**.

(b) $Z = (1, 0, 1, 0, 0, 1)$: let $t\sigma \in \Sigma_Z$. Note that the only element of $\mathbf{D}_6$ that preserves the nonzero positions is the identity; hence $\sigma = 1$. The only element $t \in \mathbf{T}^3$ that preserves these positions is the identity as well; hence Σ_Z is the trivial group.

(c) $Z = (1, 1, 1, 0, 0, 0)$: let $t\sigma \in \Sigma_Z$. Then $\sigma = 1$, and $t \in \mathbf{T}^3$ has to be $t_1 = [\frac{1}{2}, \frac{1}{2}, \frac{\pi}{2}]$ or the identity; hence $\Sigma_Z = \langle t_1 \rangle \subset \Sigma_{12}$ (from case **12**), and hence Σ_Z is not maximal.

(d) $Z = (1, 1, 0, 1, 0, 0)$: let $t\sigma \in \Sigma_Z$. Then $\sigma = 1$, and $t \in \mathbf{T}^3$ has to be the identity as well.

$\mathbf{N(Z)} = 4$. After applying $\mathbf{D}_6$, there are three possibilities for the nonzero positions. We can also make three entries equal to 1 by using a $\mathbf{T}^3$-element.

(a) $Z = (1, 1, 1, e^{2\pi i \rho}, 0, 0)$: if $t\sigma \in \Sigma_Z$, then σ is one of ξ^3, $\kappa\xi$, $\kappa\xi^4$, or 1. We conclude that $\Sigma_Z = \langle [\frac{1}{2}, \frac{1}{2}, \frac{\pi}{2}], [0, -\rho, 0]\xi^3, [-\frac{\rho}{2}, -\frac{\rho}{2}, \frac{\pi\rho}{2}]\kappa\xi \rangle$. This is conjugated to case **12** by $[0, -\frac{\rho}{2}, \frac{\pi\rho}{4}]$.

(b) $Z = (1, 0, 1, 0, 1, e^{2\pi i \rho})$: if $t\sigma \in \Sigma_Z$, then $\sigma = \kappa\xi$ or 1. $\kappa\xi Z = (1, 0, 1, 0, 1, e^{-2\pi i \rho})$, and, if Z has a nontrivial stabilizer, then t has to be a multiple of $[\frac{1}{3}, \frac{1}{3}, -\frac{\pi}{3}]$. Thus $\Sigma_Z \subset \Sigma_{10}$ (from case **10**) and hence is not maximal.

(c) $Z = (1, 0, 0, 1, 1, e^{2\pi i \rho})$: if $t\sigma \in \Sigma_Z$m, then $\sigma = \kappa\xi^4$ or 1, and $t = [\theta_1, -\theta_1, -\pi\theta_1]$ for a particular value of θ_1; hence $\Sigma_Z \subset \Sigma_{11}$ (from case **11**).

$\mathbf{N(Z)} = 5$. Such points have a trivial isotropy group.

$\mathbf{N(Z)} = 6$. Since such points have a trivial stabilizer in $\mathbf{T}^3$, the projection of Σ_Z to $\mathbf{D}_6$ is one-to-one. Thus there is a group isomorphism $\sigma \in G \mapsto \tilde{\sigma} = t_\sigma \sigma \in \Sigma_Z$, where $G \subset \mathbf{D}_6$.

Note that if $s \in \mathbf{T}^3$, then $s(t_\sigma \sigma)s^{-1} = (t_\sigma s(\sigma s^{-1}\sigma^{-1}))\sigma$. Thus we can reduce t_σ by any element in the range of $s \in \mathbf{T}^3 \mapsto s(\sigma s^{-1}\sigma^{-1}) \in \mathbf{T}^3$. The action of $\mathbf{D}_6$ by the conjugation of $\mathbf{T}^3$ is given by relations (3.2).

We classify first the isomorphisms $\mathbf{D}_6 \hookrightarrow \widetilde{\Gamma}$, up to conjugacy. Since the action of ξ on $[\theta_1, \theta_2]$ does not have 1 as an eigenvalue, one can reduce t_ξ to $[0, 0, \widehat{\phi}]$. Thus $\tilde{\xi} = [0, 0, \widehat{\phi}]\xi$. The action of κ has eigenvalue -1 in the $\widehat{\phi}$-direction. Hence, by conjugating with an element of $\mathbf{T}^3$ in this eigenspace (which commutes with ξ), we can simultaneously reduce t_κ to $[\theta_1, \theta_2, 0]$.

Let us now impose the relations of $\mathbf{D}_6$. $\tilde{\xi}^6 = 1$ implies $6\widehat{\phi} = 0$ (mod π), and the relation $\tilde{\kappa}^2 = 1$ implies $\theta_1 = 0$ (mod 1) because $\tilde{\kappa}^2 = [2\theta_1, -\theta_1, 0]$. Finally, $\tilde{\kappa}\tilde{\xi}\tilde{\kappa}\tilde{\xi} = 1$ implies $\theta_2 = 0$ (mod 1) because $\tilde{\kappa}\tilde{\xi}\tilde{\kappa}\tilde{\xi} = [-\theta_2, \theta_2, 0]$. In conclusion, up to conjugacy, there are six inclusions $\mathbf{D}_6 \hookrightarrow \widetilde{\Gamma}$, those given in cases **k=0, ... ,5**. (These cannot be conjugated by an element of $\mathbf{T}^3$ because the $\widehat{\phi}$-component of $\tilde{\xi}$ is not altered by such a conjugacy.)

It remains to establish that there are no finite maximal isotropy subgroups that are isomorphic to a proper subgroup of $\mathbf{D}_6$ and whose fixed-point subspace consists of vectors all of whose entries are nonzero. We conjecture that this statement is true, but we have not been able to prove the result.

4.7.1. Some cubic $\widetilde{\Gamma}$-equivariants.

The computation of the general $\widetilde{\Gamma}$-equivariant on $\mathbf{C}^6$ is quite complicated. Below we show that generically the dynamics on the two-dimensional fixed-point subspaces of Σ_{10} and Σ_{11} involves rotating waves and that the dynamics on Fix(Σ_{12}) can involve discrete rotating waves. To verify these statements, we need only show that certain cubic order terms in the Taylor expansion of a typical $\widetilde{\Gamma}$-equivariant are nonzero. In

this subsection, we list explicitly a few of the cubic $\widetilde{\Gamma}$-equivariants, namely, those that are sufficient to verify these statements.

Since the action of $\widetilde{\Gamma}$ on $\mathbf{C}^6$ is absolutely irreducible (see Remark 3.1), the only linear $\widetilde{\Gamma}$-equivariant is the identity map. Since $\left[0, 0, \frac{\pi}{2}\right]$ acts as $-I$ on $\mathbf{C}^6$, there are no nonzero quadratic $\widetilde{\Gamma}$-equivariants.

Since $\mathbf{D}_6$ acts transitively on the coordinates of $\mathbf{C}^6$, it follows that (cubic) equivariants are determined by their first coordinates. We claim that

(4.11)
$$(|z_2|^2 + |z_3|^2)z_1, \quad i(|z_2|^2 - |z_3|^2)z_1, \quad (z_2\overline{w}_2 + z_3\overline{w}_3)w_1, \quad |z_1|^2 z_1$$
$$(|w_2|^2 + |w_3|^2)z_1, \quad i(|w_2|^2 - |w_3|^2)z_1, \quad i(z_2\overline{w}_2 - z_3\overline{w}_3)w_1$$

are the first coordinates of $\widetilde{\Gamma}$-equivariants on $\mathbf{C}^6$. This assertion can be verified using the explicit action given in Table 3. Note that it is only necessary to check equivariance with respect to the action of $[\theta_1, \theta_2, \widehat{\phi}]$ and $\kappa\xi^3$.

4.7.2. Rotating waves. The verification that the maximal isotropy subgroups Σ_{10} and Σ_{11} lead to rotating waves on the hexagonal lattice is identical to the verification that the isotropy subgroup Σ_5 on the square lattice leads to rotating waves, as shown in section 4.4. All that needs to be shown is that there is a cubic equivariant whose restriction to $\mathrm{Fix}(\Sigma_{10})$ is $i|u|^2 u$. For example, we may take the equivariant whose first coordinate is $i(|z_2|^2 - |z_3|^2)z_1$. Similarly, the equivariant whose first coordinate is $i(|w_2|^2 - |w_3|^2)z_1$ restricts to $i|u|^2 u$ on $\mathrm{Fix}(\Sigma_{11})$. The group orbit along which the rotating wave travels is given by the normalizer of the isotropy subgroup Σ, and that information is given in Table 4.

4.7.3. Discrete rotating wave: $\Sigma_{12} = \langle \kappa\xi, \xi^3, [\frac{1}{2}, \frac{1}{2}, \frac{\pi}{2}] \rangle$. Any $\widetilde{\Gamma}$-equivariant vector field restricted to $\mathrm{Fix}(\Sigma_{12}) \cong \mathbf{C}$ is $\mathbf{Z}_4$-equivariant since $N(\Sigma_{12})/\Sigma_{12} \cong \mathbf{Z}_4$. See Table 4. It follows that the restricted vector field has the form

(4.12)
$$f(u) = A(|u|^2, u^4)u + B(|u|^2, u^4)\overline{u}^3,$$

where A and B are complex-valued functions. To cubic order

$$f(u, \lambda) = (\lambda + a|u|^2)u + b\overline{u}^3,$$

where $\lambda, a, b \in \mathbf{C}$. In fact, absolute irreducibility of the action of $\widetilde{\Gamma}$ implies that $\lambda \in \mathbf{R}$. For $\lambda \neq 0$, we rescale time t so that $\lambda = 1$. If $b \neq 0$, then after rescaling u to αu, where $\alpha \in \mathbf{C}$, we can assume that $b = 1$ and that λ is unchanged. Krauskopf [18, 19] classified the dynamical states that the cubic truncation can exhibit for all b and λ; these states include equilibria and time-periodic orbits even when $\lambda = 1$. For periodic states, see [18, p. 1086, Figure 12 (between regions 14 and 15)]. Normal hyperbolicity of these solutions guarantees that the equilibria

and periodic states persist as solutions in (4.12). Note that $|z_1|^2 z_1$ and $i(|z_2|^2 - |z_3|^2)z_1$ are the first coordinates of $\widetilde{\Gamma}$-equivariants on $\mathbf{C}^6$ whose restrictions to $\text{Fix}(\Sigma_{12})$ are $|u|^2 u$ and $i|u|^2 u$. To complete this proof, we need to find $\widetilde{\Gamma}$-equivariant cubics that restrict to $\overline{u}^3$ and $i\overline{u}^3$ on $\text{Fix}(\Sigma_{12})$. The first coordinates of such cubics are $(z_2\overline{w}_2 + z_3\overline{w}_3)w_1$ and $i(z_2\overline{w}_2 - z_3\overline{w}_3)w_1$.

4.8. Effect of weak anisotropy on hexagonal lattice. We now present the details of the effect of forced symmetry-breaking on each of the 12 types of solutions that correspond to maximal isotropy subgroups on the hexagonal lattice.

The strategy is the same as in section 2.4: given a (relative) equilibrium of a $\widetilde{\Gamma}$-equivariant flow, consider its orbit under the connected component of $\widetilde{\Gamma}$, a 3-torus. This set (which is a torus of dimension at most 3) is invariant under the flow. Assuming that this set is normally hyperbolic, Lemma 4.2 guaranties that small Γ-equivariant perturbations of the flow still admit a nearby invariant set, diffeomorphic to that of the unperturbed flow. Since this diffeomorphism can be made Γ-equivariant, we can analyze the effect of breaking the $\widehat{\phi}$-symmetry on the unperturbed torus itself. We base our analysis on symmetry considerations, namely, intersections of this torus with fixed-point spaces. These determine flow-invariant sets: when these are points, they are equilibria, whereas if they are higher-dimensional, then one expects that generically the flow is nontrivial. This approach is used by Lauterbach and Roberts [20] in their analysis of forced symmetry-breaking.

We use two assumptions to draw our conclusions: the flow-invariant toral sets described above are generically normally hyperbolic for a $\widetilde{\Gamma}$-equivariant flow, and, after breaking the isotropy, the Γ-invariant flow is generically nontrivial whenever the Γ-symmetry *on the invariant torus* allows it.

Note that normal hyperbolicity is generic. For the case of the square lattice, we computed the general form of a $\widetilde{\Gamma}$-equivariant flow and concluded that, for various parameter choices, the invariant sets corresponding to the five maximal isotropy subgroups can each be attractive. See section 4.5. We expect the same to be true in the case of the hexagonal lattice. However, the computations are tedious, and we did not perform them.

To address the other assumption, we must either compute the general form of the Γ-equivariant perturbation of a $\widetilde{\Gamma}$-equivariant vector field and show that it permits vector fields that are nonzero on the sets under consideration or show that certain Γ-equivariant vector fields on the toral sets introduced above can be extended to Γ-equivariant vector fields on $\mathbf{C}^6$.

4.8.1. The family $\Sigma_{k+1} = \mathbf{D}_6(\kappa, [0, 0, \frac{k\pi}{2}]\xi)$, $k = 0, \ldots, 5$. Each of these subgroups is axial, with the fixed-point subspace spanned, respectively, by

$$v_k = (v^{3k}, v^{3k}, v^{7k}, v^{11k}, v^{11k}, v^{7k}), \quad v = e^{i\frac{\pi}{6}}.$$

In the isotropic case, the flow-invariant group orbit is a 3-torus $\mathbf{T}_k^3$ obtained by applying $[\theta_1, \theta_2, \widehat{\phi}]$ to the point v_k. When the anisotropy is small, there still exists a flow-invariant set close to the 3-torus described above. The flow on this set can be understood by analyzing the isotropic case. In the following, we consider Γ-equivariant flows on this 3-torus. To simplify notation, we sometimes drop the reference to k.

Each of these 3-tori is foliated by 2-tori $T_{\widehat{\phi}} = T_{k,\widehat{\phi}}$ that are swept out by the action of $[\theta_1, \theta_2, 0]$ on $[0, 0, \widehat{\phi}]v_k$. By $[\theta_1, \theta_2]$-equivariance, the flow on these 2-tori is parallel. Certain of the 2-tori $T_{\widehat{\phi}}$ are forced by Γ-symmetry to be flow-invariant; we call them *critical*. Generically, other than the critical 2-tori, there are only finitely many other 2-tori that are flow-invariant. We expect the flow between the invariant 2-tori to be transverse to the noninvariant $T_{\widehat{\phi}}$'s.

If $k \neq 1, 5$, the invariant 2-tori consist of fixed points, and on the 3-torus T_k^3 the flow is along the curves $[\theta_1, \theta_2] = $ constant. For $k = 1, 5$, the flow on the invariant 2-tori is generically expected to be nontrivial (and parallel, as discussed above). For each critical torus, the direction of the flow can be determined explicitly. See Table 9.

Table 9

Conjugacy classes of critical $T_{\widehat{\phi}}$'s and flows on them. When flow is nontrivial, the direction of flow $[\theta_1, \theta_2]$ is given. When equilibrium is scalar or pseudoscalar, that is denoted by $W_1^\pm$. ℓ denotes the number of conjugacy classes in Γ of each critical torus, and $v = [0, 0, \widehat{\phi}]v_k$ is the point where the isotropy subgroup $\Sigma_v \subset \Gamma$ is computed.

k	$\widehat{\phi}$	$[\theta_1, \theta_2]$ or $W_1^\pm$	Σ_v	$\widehat{\phi}$	$[\theta_1, \theta_2]$ or $W_1^\pm$	Σ_v	ℓ
0	0	W_1^+	$\mathbf{D}_6(\kappa, \xi)$	$\frac{\pi}{2}$	W_1^+	$\mathbf{D}_6(\kappa, \xi)$	1
1	0	$[-2\theta_2, \theta_2]$	$\mathbf{D}_1(\kappa)$	$\frac{\pi}{12}$	$[-\theta_2, \theta_2]$	$\mathbf{D}_1(\kappa\xi)$	6
2	0		$\mathbf{D}_2(\kappa, \xi^3)$	$\frac{\pi}{2}$		$\mathbf{D}_2(\kappa, \xi^3)$	3
3	0	W_1^+	$\mathbf{D}_3(\kappa, \xi^2)$	$\frac{\pi}{4}$	W_1^-	$\mathbf{D}_3(\kappa\xi, \xi^2)$	2
4	0		$\mathbf{D}_2(\kappa, \xi^3)$	$\frac{\pi}{2}$		$\mathbf{D}_2(\kappa, \xi^3)$	3
5	0	$[-2\theta_2, \theta_2]$	$\mathbf{D}_1(\kappa)$	$\frac{\pi}{12}$	$[\theta_1, 0]$	$\mathbf{D}_1(\kappa\xi^5)$	6

We now present the details needed to derive the information in Table 9. For $\sigma \in \Gamma$, we are interested in the intersection of $\text{Fix}(\sigma)$ with the 3-torus $\mathbf{T}_k^3$ swept out by v_k under the action of $[\theta_1, \theta_2, \widehat{\phi}]$.

This intersection is nontrivial only if the isotropy subgroup of a point in $\mathbf{T}_k^3$ contains σ. However, these isotropy subgroups are easy to compute because we know the isotropy subgroup of v_k:

$$\Sigma_{v_k} = \langle \kappa, \widetilde{\xi} \rangle \cong \mathbf{D}_6,$$

where $\widetilde{\xi} = \left[0, 0, \frac{k\pi}{6}\right]\xi$.

Hence the isotropy subgroup of $[\theta_1, \theta_2, \widehat{\phi}]v_k$ is given by $[\theta_1, \theta_2, \widehat{\phi}]\Sigma_{v_k}[-\theta_1, -\theta_2, -\widehat{\phi}]$. It

follows from (3.2) that for $\tilde{\sigma} = \kappa^\varepsilon \tilde{\xi}^p \in \Sigma_{v_k}$ ($\varepsilon \in \{0,1\}$, $p = 0, \ldots, 5$),

$$
(4.13) \qquad [\theta_1, \theta_2, \widehat{\phi}] \tilde{\sigma} [-\theta_1, -\theta_2, -\widehat{\phi}] = \left[(I - A_\sigma) \begin{pmatrix} \theta_1 \\ \theta_2 \end{pmatrix}, 2\varepsilon\widehat{\phi} + (-1)^\varepsilon \frac{pk\pi}{6} \right] \sigma,
$$

where $\sigma = \kappa^\varepsilon \xi^p$ and A_σ is the action by conjugation of $\sigma \in \mathbf{D}_6$ on $[\theta_1, \theta_2]$ (see (3.2)), and

$$
\kappa[\theta_1, \theta_2] = [\theta_1, -\theta_1 - \theta_2]\kappa,
$$
$$
\xi[\theta_1, \theta_2] = [-\theta_2, \theta_1 + \theta_2]\xi.
$$

Hence

$$
A_\kappa = \begin{pmatrix} 1 & 0 \\ -1 & -1 \end{pmatrix}, \qquad A_\xi = \begin{pmatrix} 0 & -1 \\ 1 & 1 \end{pmatrix}.
$$

For $\sigma = \kappa^\varepsilon \xi^p$ and $0 \leq \eta_1, \eta_2 \leq 1$, we conclude that

$$
(4.14) \qquad \mathrm{Fix}([\eta_1, \eta_2, 0]\sigma) \cap \mathbf{T}_k^3 = \{[\theta_1, \theta_2, \widehat{\phi}]v_k : \theta_1, \theta_2, \widehat{\phi} \text{ satisfies } (4.15), (4.16)\},
$$

where

$$
(4.15) \qquad (I - A_\sigma) \begin{pmatrix} \theta_1 \\ \theta_2 \end{pmatrix} = \begin{pmatrix} \eta_1 \\ \eta_2 \end{pmatrix},
$$

$$
(4.16) \qquad 2\varepsilon\widehat{\phi} + (-1)^\varepsilon \frac{pk\pi}{6} = 0 \ (\mathrm{mod} \ \pi).
$$

Each of these intersections is flow-invariant and one-dimensional unless it is empty or $\mathbf{T}_k^3$ (as one can check by computing the A_σ's). We now consider separately the two cases, determined by whether or not k is relatively prime to 6.

$k = 1, 5$. Equation (4.16) cannot be satisfied if $\varepsilon = 0$; hence the intersections are trivial for $\sigma = \xi^p$, $p \neq 0$. For $\varepsilon = 1$, (4.16) gives $2\widehat{\phi} = \frac{pk\pi}{6}$ (mod π); note that different values of p give different values of $\widehat{\phi}$, and hence different elements of Γ produce disjoint intersections with $\mathbf{T}_k^3$. These are the critical 2-tori. Since $I - A_{\kappa\xi^p}$ has rank one, (4.15) gives a flow-invariant line in the corresponding $T_{\widehat{\phi}}$.

$k = 0, 2, 3, 4$. Setting $\varepsilon = 1$ and $p = 0, \ldots, 5$, we find the finite set of critical $\widehat{\phi}$-values from (4.16). Choose a value $p \neq 0$ such that $pk \equiv 0$ (mod 6). Then, for $\sigma = \xi^p$, the intersection (4.14) is given by circles with constant $[\theta_1, \theta_2]$, because the rank of $I - A_{\kappa\xi^p}$ is equal to 2. Since these flow-invariant circles intersect each $T_{\widehat{\phi}}$ transversely, the flow has to be trivial on the invariant $T_{\widehat{\phi}}$'s. Note that A_σ gives the only faithful two-dimensional representation of $\mathbf{D}_6$. This explains the values of $\mathrm{rank}(I - A_\sigma)$.

We decide now which critical 2-tori are conjugate by Γ. (Since the field is Γ-equivariant, the action of Γ permutes the invariant 2-tori $T_{\widehat{\phi}}$.) Relation (4.13) shows that

$$\kappa^\varepsilon \xi^{p'} T_{\widehat{\phi}} = T_{\widehat{\psi}}, \quad \text{where} \quad \widehat{\psi} = (-1)^\varepsilon \left(\widehat{\phi} - \frac{p'k\pi}{6} \right) \ (\text{mod } \pi).$$

Solving (4.16) with $\varepsilon = 1$ for the critical values of $\widehat{\phi}$, we see that for each k there are two Γ-conjugacy classes of critical tori $T_{\widehat{\phi}}$ in $\mathbf{T}_k^3$.

4.8.2. $\Sigma_7 = \langle \kappa \xi^3, [0, \theta_2, 0], [\theta_1, 0, -\pi\theta_1] \rangle$. Equilibria of type Σ_7 appear in circles. When symmetry breaks, we see that $(\pm 1, 0, 0, 0, 0, 0)$ must remain as equilibria, since these points form the intersection of $\text{Fix}(\kappa\xi^3)$ with the circle $(z_1, 0, 0, 0, 0, 0)$, where $|z_1| = 1$. Since $[\theta_1, 0, 0]$ acts transitively on the circle, all points on the circle are equilibria.

4.8.3. $\Sigma_8 = \langle \kappa, \xi^3, [0, \theta_2, 0], [\frac{1}{2}, 0, \frac{\pi}{2}] \rangle$. Equilibria of type Σ_8 lie on the 2-torus $(z_1, w_1, 0, 0, 0, 0)$, where $|z_1| = |w_1| = 1$. The following group elements act on this torus:

$$
\begin{aligned}
[\theta_1, 0, 0](z_1, w_1) &= (e^{-2\pi i \theta_1} z_1, e^{-2\pi i \theta_1} w_1), \\
\kappa(z_1, w_1) &= (w_1, z_1), \\
\xi^3(z_1, w_1) &= (\overline{w}_1, \overline{z}_1), \\
\kappa\xi^3(z_1, w_1) &= (\overline{z}_1, \overline{w}_1).
\end{aligned}
$$

Note that $\text{Fix}(\mathbf{D}_2)$ intersects the 2-torus at two points $(1, 1)$ and $(-1, -1)$. Thus these two points are fixed in the anisotropic case. Moreover, $\text{Fix}(\kappa)$ is the circle $z_1 = w_1$ on the torus, and it must be flow-invariant. Since $[\theta_1, 0, 0]$ acts on that circle, the points on the circle are conjugate and must also be fixed points of the flow.

Next note that $\text{Fix}(\kappa\xi^3)$ consists of four points $(\pm 1, \pm 1)$. Thus the circle generated by $[\theta_1, 0, 0]$ through $(1, -1)$ also consists of fixed points. Finally, note that $\text{Fix}(\xi^3)$ is a circle perpendicular to the diagonal (z_1, z_1) and is also flow-invariant. Thus $[\theta_1, 0, 0]$-symmetry implies that the dynamics on the 2-torus is along circles perpendicular to the diagonal and that each such circle has four equilibria (two pairs of conjugate equilibria).

We can assume that (up to symmetry) in the anisotropic case there are two kinds of equilibria corresponding to type Σ_8, namely, $(1, 1, 0, 0, 0, 0)$ and $(1, -1, 0, 0, 0, 0)$. These correspond to scalar and pseudoscalar rolls.

4.8.4. $\Sigma_9 = \langle \xi^2, \kappa\xi, [\frac{1}{3}, \frac{1}{3}, \frac{2\pi}{3}] \rangle$. The group orbits for equilibria of type Σ_9 are 3-tori modeled by $|z_1| = |z_2| = |z_3| = 1$. In the anisotropic case, there are seven flow-invariant circles on this $\mathbf{T}^3$ and two fixed points. The fixed points are given by $\text{Fix}(\mathbf{D}_3(\xi^2, \kappa\xi)) = \pm(1, 1, 1)$. $\text{Fix}(\xi^2)$ gives one of the circles $z_1 = z_2 = z_3$, and each of $\text{Fix}(\kappa\xi)$, $\text{Fix}(\kappa\xi^3)$, and $\text{Fix}(\kappa\xi^5)$ gives two invariant circles. Although the dynamics on this group orbit seems complicated to describe, we know that we will get at least two fixed points corresponding to $\pm(1, 0, 1, 0, 1, 0)$.

4.8.5. $\Sigma_{10} = \langle \kappa\xi, [\theta_1, \theta_1, -\pi\theta_1] \rangle$. In the isotropic case, solutions corresponding to the maximal isotropy subgroup of type Σ_{10} can be expected to be a rotating wave, since its fixed-point subspace is two-dimensional and the normalizer of the isotropy subgroup acts as a circle on this fixed-point subspace. See section 4.7.2. We claim that the same is true in the anisotropic case.

Observe that the group orbit of solutions is the 2-torus $(z_1, 0, z_2, 0, 0, 0)$, where $|z_1| = 1 = |z_2|$. Observe that

$$\kappa\xi(z_1, z_2) = (\bar{z}_2, \bar{z}_1).$$

Note that $[\theta_1, \theta_2, 0]$ acts transitively on the 2-torus so that the flow on the 2-torus is a linear flow. Finally, note that $\text{Fix}(\kappa\xi) = \{(z_1, \bar{z}_1)\}$ is a circle $\rho_1 + \rho_2 = 0$, where $z_j = e^{2\pi i \rho_j}$. So this circle (and all circles parallel to it on the 2-torus) are flow-invariant and rotating waves.

4.8.6. $\Sigma_{11} = \langle \kappa\xi^4, [\theta_1, -\theta_1, -\pi\theta_1] \rangle$. The analysis of the maximal isotropy subgroup of type Σ_{11} is identical to that of Σ_{10}, and, in the anisotropic case, group orbits are 2-tori foliated by flow-invariant traveling waves. Note that the invariant circles $\text{Fix}(\kappa\xi^4)$ are parallel to the main diagonal $z_1 = w_2$.

4.8.7. $\Sigma_{12} = \langle \xi^3, \kappa\xi, [\frac{1}{2}, \frac{1}{2}, \frac{\pi}{2}] \rangle$. We now describe what happens to the discrete rotating wave associated to the isotropy subgroup Σ_{12} (discussed in section 4.7.3) when symmetry-breaking terms are added. The main mathematical issue is that $\text{Fix}(\Sigma_{12})$ is no longer flow-invariant when symmetry-breaking terms are added. Since the symmetry group of the discrete rotating wave is finite, the action of the connected component of $\widetilde{\Gamma}$ on this periodic solution yields an invariant 4-torus, which is preserved by normal hyperbolicity. However, the three-dimensional invariant subspace

$$W = \text{Fix}(\langle \xi^3, \kappa\xi \rangle) = \{(u, \bar{u}, \bar{u}, u, x, x) \mid u \in \mathbf{C}, x \in \mathbf{R}\} \supset \text{Fix}(\Sigma_{12})$$

survives symmetry-breaking. It is straightforward to check that the intersection of the 4-torus with W is the original periodic solution. Therefore, the periodic state will survive small symmetry-breaking terms and remain in W.

REFERENCES

[1] A. ANGELUCCI, J. B. LEVITT, AND J. S. LUND, *Anatomical origins of the classical receptive field and modulatory surround field of single neurons in macaque visual cortical area*, in Changing Views of Cajal's Neuron, Progress in Brain Research 136, Elsevier, Amsterdam, 2002, pp. 373–388.

[2] G. G. BLASDEL, *Orientation selectivity, preference, and continuity in monkey striate cortex*, J. Neurosci., 12 (1992), pp. 3139–3161.

[3] I. BOSCH VIVANCOS, P. CHOSSAT, AND I. MELBOURNE, *New planforms in systems of partial differential equations with Euclidean symmetry*, Arch. Rational Mech. Anal., 131 (1995), pp. 199–224.

[4] W. H. BOSKING, Y. ZHANG, B. SCHOFIELD, AND D. FITZPATRICK, *Orientation selectivity and the arrangement of horizontal connections in tree shrew striate cortex*, J. Neurosci., 17 (1997), pp. 2112–2127.

[5] P. C. BRESSLOFF, J. D. COWAN, M. GOLUBITSKY, AND P. J. THOMAS, *Scalar and pseudoscalar bifurcations motivated by pattern formation on the visual cortex*, Nonlinearity, 14 (2001), pp. 739–775.

[6] P. C. BRESSLOFF, J. D. COWAN, M. GOLUBITSKY, P. J. THOMAS, AND M. C. WIENER, *Geometric visual hallucinations, Euclidean symmetry, and the functional architecture of striate cortex*, Phil. Trans. Royal Soc. London B, 356 (2001), pp. 299–330.

[7] P. C. BRESSLOFF, J. D. COWAN, M. GOLUBITSKY, P. J. THOMAS AND M. C. WIENER, *What geometric visual hallucinations tell us about the visual cortex*, Neural Computation, 14 (2002), pp. 473–491.

[8] J. D. COWAN, *Some Remarks on channel bandwidths for visual contrast detection*, Neurosciences Research Program Bull., 15 (1977), pp. 492–517.

[9] G. B. ERMENTROUT AND J. D. COWAN, *A mathematical theory of visual hallucination patterns*, Biol. Cybernetics, 34 (1979), pp. 137–150.

[10] U. EYSEL, *Turning a corner in vision research*, Nature, 399 (1999), pp. 641–644.

[11] M. FIELD AND J. W. SWIFT, *Stationary bifurcation to limit cycles and heteroclinic cycles*, Nonlinearity, 4 (1991), pp. 1001–1043.

[12] C. D. GILBERT, *Horizontal integration and cortical dynamics*, Neuron, 9 (1992), pp. 1–13.

[13] M. GOLUBITSKY AND I. STEWART, *The Symmetry Perspective: From Equilibrium to Chaos in Phase Space and Physical Space*, Progr. Math., 200, Birkhäuser, Basel, 2002.

[14] M. GOLUBITSKY, I. STEWART, AND D. G. SCHAEFFER, *Singularities and Groups in Bifurcation Theory: Vol.* II, Appl. Math. Sci. 69, Springer-Verlag, New York, 1988.

[15] M. HIRSCH, C. PUGH, AND M. SHUB, *Invariant Manifolds*, Lecture Notes in Math 583, Springer-Verlag, New York.

[16] D. H. HUBEL AND T. N. WIESEL, *Sequence regularity and geometry of orientation columns in the monkey striate cortex*, J. Comp. Neurol., 158 (1974), pp. 267–294; *Uniformity of monkey striate cortex: a parallel relationship between field size, scatter, and magnification factor*, J. Comp. Neurol., 158 (1974), pp. 295–306; *Ordered arrangement of orientation columns in monkeys lacking visual experience*, J. Comp. Neurol., 158 (1974), pp. 307–318.

[17] H. KLÜVER, *Mescal and Mechanisms of Hallucinations*, University of Chicago Press, Chicago, 1966.

[18] B. KRAUSKOPF, *Bifurcation sequences at 1:4 resonance: An inventory*, Nonlinearity, 7 (1994), pp. 1073–1091.

[19] B. KRAUSKOPF, *The bifurcation set for the 1:4 resonance problem*, Experiment. Math., 3 (1994), pp. 107–128.

[20] R. LAUTERBACH AND M. ROBERTS, *Heteroclinic cycles in dynamical systems with broken spherical symmetry*, J. Differential Equations, 100 (1992), pp. 22–48.

[21] I. MELBOURNE, *Maximal isotropy subgroups for absolutely irreducible representations of compact Lie groups*, Nonlinearity, 7 (1994), pp. 1385–1393.

[22] E. SCHWARTZ, *Spatial mapping in the primate sensory projection: Analytic structure and relevance to projection*, Biol. Cybernetics, 25 (1977), pp. 181–194.

[23] L. C. SINCICH AND G. G. BLASDEL, *Oriented axon projections in primary visual cortex of the monkey*, J. Neurosci., 21 (2001), pp. 4416–4426.

[24] P. TASS, *Oscillatory cortical activity during visual hallucinations*, J. Biol. Phys., 23 (1997), pp. 21–66.

[25] H. R. WILSON AND J. D. COWAN, *Excitatory and inhibitory interactions in localized populations of model neurons*, Biophys. J., 12 (1972), pp. 1–24.

[26] F. WOLF AND T. GEISEL, *Spontaneous pinwheel annihilation during visual development*, Nature, 395 (1998), pp. 73–78.